Cyclic-N_3. II. Significant geometric phase effects in the vibrational spectra

Dmitri Babikov
Chemistry Department, Marquette University, Wehr Chemistry Building, Milwaukee, Wisconsin 53201

Brian K. Kendrick
Theoretical Chemistry and Molecular Physics (T-12), Los Alamos National Laboratory, Los Alamos MS B268, New Mexico 87545

Peng Zhang and Keiji Morokuma
Department of Chemistry, Emory University, Chemistry Building, Atlanta, Georgia 30322

(Received 30 July 2004; accepted 5 October 2004; published online 11 January 2005)

An accurate theoretical prediction of the vibrational spectra for a pure nitrogen ring (cyclic-N_3) molecule is obtained up to the energy of the $^2A_2/^2B_1$ conical intersection. A coupled-channel approach using the hyperspherical coordinates and the recently published *ab initio* potential energy surface [D. Babikov, P. Zhang, and K. Morokuma, J. Chem. Phys. **121**, 6743 (2004)] is employed. Two independent sets of calculations are reported: In the first set, the standard Born–Oppenheimer approximation is used and the geometric phase effects are totally neglected. In the second set, the generalized Born–Oppenhimer approximation is used and the geometric phase effects due to the D_{3h} conical intersection are accurately treated. All vibrational states are analyzed and assigned in terms of the normal vibration mode quantum numbers. The magnitude of the geometric phase effect is determined for each state. One important finding is an unusually large magnitude of the geometric phase effects in the cyclic-N_3: it is $\sim 100\ cm^{-1}$ for the low-lying vibrational states and exceeds 600 cm^{-1} for several upper states. On average, this is almost two orders of magnitude larger than in the previously reported studies. This unique example suggests a favorable path to experimental validation. © *2005 American Institute of Physics*. [DOI: 10.1063/1.1824905]

I. INTRODUCTION

The previously unknown energetic form of nitrogen has been recently predicted theoretically[1] and produced experimentally.[2–5] This is a stable ring-N_3 isomer (having the form of an isosceles triangle) called cyclic-N_3 hereafter. Cyclic-N_3 is metastable with respect to dissociation to the ground state $N(^4S)+N_2$ ($\Delta E=-1.4$ eV), which is spin forbidden. Furthermore, recent results[6] show that the doublet-quartet surface crossings that must be traversed for dissociation lie about 1 eV above the cyclic-N_3 minimum. Thus, cyclic-N_3 is very stable and carries a lot of energy; it is an excellent new candidate for technological applications in energy storage, high nitrogen explosives, and clean propellants. It is worth mentioning that the nitrogen resources on our planet are practically limitless.

The cyclic-N_3 is a new molecule and experimental studies of it have been somewhat ahead of theory. Valuable theoretical guidance for designing experiments and for interpreting experimental results has been notably lacking during the last couple years. This paper is the second one in a series of theoretical papers we intend to publish which focus on cyclic-N_3. In the first paper,[7] we presented an accurate *ab initio* potential energy surface (PES) for cyclic-N_3. Cyclic-N_3 is a Jahn–Teller molecule that exhibits a conical intersection between two of its potential energy surfaces at the D_{3h} (equilateral triangle) configuration.[6,7] That conical intersection causes the equilibrium geometry to distort off the D_{3h} geometry. In the present paper, we report calculations of the vibrational states of cyclic-N_3 with particular emphasis on the associated geometric phase effects.

The origin of the geometric phase dates back to 1963 when Herzberg and Longuet-Higgins[8] showed that a Born–Oppenheimer electronic wave function changes sign for any closed path in the nuclear parameter space which encircles a conical intersection of two electronic PESs. The geometrical interpretation of the sign change was first recognized by Mead and Truhlar[9] in 1979. They showed that the sign change can be expressed in terms of the "magnetic flux" due to a pseudomagnetic solenoid centered at the degeneracy point. Later, Mead[10] called this effect the "molecular Aharonov–Bohm" effect. In 1984, Berry[11] showed that the sign change was a special case of a more general geometric phase factor often referred to as "Berry's phase." Due to the universal nature of this effect, Berry's influential paper generated widespread interest which continues to this day.

As noted by Ham,[12] probably the first experimentally verified example of a geometric phase effect was in crystal defects with strong Jahn–Teller coupling where the lowest vibronic state was shown to have E symmetry instead of A_1 or A_2.[13] The first experimental verification of this ordering was for Cu^{2+} in MgO using electronic paramagnetic resonance (EPR).[14] This ordering is a direct consequence of the geometric phase. If it were not properly included, the opposite ordering would be predicted (i.e., the lowest vibronic state would be A_1 or A_2).

The theoretical treatment of geometric phase effects in molecular spectra date back to Longuet–Higgins *et al.*[15] who

correctly included the geometric phase in a model of a Jahn-Teller distorted molecule. The first calculations to treat a real molecule (Li_3) were performed by Gerber and Schumacher.[16] The vibrational spectra of Cu_3 both in an excited electronic state and in its ground state have also been computed.[17,18] As expected, the lowest vibrational state for these systems was found to be of E symmetry. Significant geometric phase effects were also found in the vibrational spectra of $Na_3(X)$.[19,20] The geometric phase shifts many of the vibrational energies (relative to a calculation which ignores the geometric phase). These energy shifts result in a reordering of many of the vibrational levels which can be confirmed experimentally. Similar calculations for Na_3 in an excited electronic state found significant geometric phase effects which were confirmed experimentally.[21] A similar treatment for Li_3 also confirmed the effects of the geometric phase in the vibrational spectra associated with both the ground and an excited electronic state.[22] Other theoretical studies of geometric phase effects in molecular spectra can be found in Refs. 23–26. Geometric phase effects have also been reported in quantum reactive scattering calculations. The first calculation of this kind dates back to 1990 by Lepetit and Kuppermann.[27] For a detailed review of these kinds of calculations see the recent review articles by Kendrick.[28,29] More discussion of geometric phase effects in molecules can also be found the in the review articles by Mead[30] and Yarkony.[31]

In the generalized Born–Oppenheimer (GBO) approach of Mead and Truhlar,[9] the double-valued real electronic wave function is multiplied by a complex phase factor. This phase factor is chosen to exactly cancel the sign change associated with the double-valued real electronic wave function so that the resulting complex electronic wave function is single valued. However, the effective Schrödinger equation for the nuclear motion acquires a vector potential (or gauge potential) and is more difficult to solve. In recent years this method of incorporating the geometric phase effects into accurate quantum mechanical calculations has been applied to several inelastic and reactive scattering problems[32–36] as well as to calculations of the vibrational spectra in the Na_3 triatomic molecule.[19,20] In the present paper we follow this approach too.

In Sec. II of the paper we briefly review the properties of the cyclic-N_3 PES and demonstrate how the electronic wave function of cyclic-N_3 changes sign when the nuclear motion encircles the conical intersection, which is the origin of the geometric phase effects. In Sec. III we review both the standard BO and the generalized BO approaches to calculations of the vibrational spectra. In Sec. IV we describe numerical techniques used in this work to solve the Schrödinger equation for the nuclear motion. The results of the BO and the GBO calculations are presented in Secs. V and VI, respectively. In Sec. VII we highlight the geometric phase effects found in cyclic-N_3, and some conclusions are presented in Sec. VIII.

II. POTENTIAL ENERGY SURFACE

In this work we use a sophisticated adiabatic PES for the ground doublet electronic state of the cyclic-N_3.[7] It is based on extensive electronic structure calculations using the MOLPRO 2002.6 suite of *ab initio* programs.[37] Dunning's standard correlation consistent polarized valence triple-ζ basis set augmented with diffuse functions (aug-cc-pVTZ) was used and the internally contracted multireference configuration interaction method with all singles and doubles (MRCISD) wave functions[38] was employed. To all MRCISD energies the multireference version of the Davidson correction[39] was applied that can be denoted as MRCISD(Q). In the MRCISD(Q) calculations, the reference wave function was obtained from the corresponding full valence CASSCF calculations consisting of 15 electrons distributed in 12 molecular orbitals, and only the $1s$ orbitals of N atoms were kept doubly occupied in all configurations while the remaining 15 electrons were correlated, denoted as MRCISD(Q) $(15e/12o)$ aug-cc-pVTZ.

As in Ref. 7, we describe the positions of nitrogen nuclei in the cyclic-N_3 triatomic using adiabatically adjusting principal-axes hyperspherical (APH) coordinates.[40,41] In terms of the usual mass scaled internal Jacobi coordinates (r,R,α) the APH coordinates (ρ,θ,ϕ) are defined as follows:

$$\rho=\sqrt{R^2+r^2}, \quad \rho\in[0;\infty], \tag{1}$$

$$\tan\theta=\frac{\sqrt{(R^2-r^2)^2+(2Rr\cos\alpha)^2}}{2Rr\sin\alpha}, \quad \theta\in[0;\pi/2], \tag{2}$$

$$\tan\phi=\frac{2Rr\cos\alpha}{R^2-r^2}, \quad \phi\in[0;2\pi]. \tag{3}$$

Qualitatively, the value of the hyperradius ρ is a measure of the overall "size" of a triatomic molecule. Hyperangles θ and ϕ describe changes in its "shape."

Often used with APH coordinates is the stereographic projection,[40] which is a convenient way to plot a two-dimensional (2D) slice of the PES at a fixed value of the hyperradius ρ, while θ and ϕ are allowed to vary. This corresponds to variation of the shape of the triatomic keeping its overall size constant. In such a 2D plot the energy is a function of two Cartesian variables X and Y defined as

$$X=\cos\phi\tan(\theta/2), \tag{4}$$

$$Y=\sin\phi\tan(\theta/2), \tag{5}$$

where $-1\leqslant X\leqslant 1$, $-1\leqslant Y\leqslant 1$. With such a choice the center of the plot $(X=0, Y=0)$ corresponds to $\theta=0$ and describes the triatomic in D_{3h} geometry (equilateral triangle). A distance of any point from the center of the plot is determined by the θ variable only:

$$\sqrt{X^2+Y^2}=\tan(\theta/2). \tag{6}$$

Points at the unit circle $X^2+Y^2=1$ correspond to $\theta=\theta_{\max}=\pi/2$ and describe linear configurations of the N_3 triatomic system (not studied in this paper). Stereographic projections will be used many times throughout the following section.

Using APH coordinates we have set up a dense (ρ,θ,ϕ) grid in three dimensions. In Ref. 7 we had 18 points in ρ covering the range from 3.19 to 3.93 a.u. 18 points in θ covering the range from zero to $\tan(\theta/2)=0.25$; and seven points covering the whole range of ϕ (from zero to 60°).

Electronic structure calculations were performed for all geometries on this grid, which resulted in the 2286 *ab initio* points determined in Ref. 7. Convergence studies performed in this work have shown that the vibrational wave function of N_3 tunnels deep into the classically forbidden region and the grid should be slightly extended onto the range of small ρ values as well as onto the range of large θ values. Consequently, we have added to the grid of Ref. 7 an additional ρ point at $\rho=3.18$ a.u. and an additional θ point at $\tan(\theta/2)=0.29$, which resulted in 260 additional *ab initio* points on 3D-grid computed for this work. Finally, an accurate three-dimensional interpolant has been constructed between the *ab initio* points using the tensor product *B*-cubic spline representation.[42]

All features of the PES were described in detail in Ref. 7. In this paper, we give only a brief summary of the PES's major features. The crossing of the potential energy surfaces for $^2A_2$ and $^2B_1$ electronic states in cyclic-N_3 forms a seam along the ρ axis ($\theta=0$, $\phi=0$), which is the D_{3h} symmetry line in the APH coordinates. Therefore, for each value of ρ the conical intersection is at the origin ($X=0$, $Y=0$) and is surrounded by a deep attractive well, as shown in Fig. 1(a). At the bottom of the well there are three equilibrium minima at $\phi=\{0; 120°; 240°\}$ separated by the three low energy transition states at $\phi=\{60°; 180°; 300°\}$, as seen in Fig. 1(b). The three minima correspond to the three possible permutations of nitrogen nuclei within the cyclic-N_3 triatomic. They have the same energy and this energy is taken as the energy reference point throughout the paper. Relative to it the energy of the transition state points or pseudorotation barrier is only 311.33 cm^{-1}. The energy of the conical intersection depends upon the size of equilateral triangle and is a smooth function of the hyperradius ρ. It exhibits a minimum at $\rho=3.4070$ a.u. where the energy is 4599.28 cm^{-1}. This point will be referred as the minimum energy point of the conical intersection.

In the APH coordinates, all geometries of an X_3 triatomic molecule with $\phi=n\times 60°$ (n is an integer) belong to the C_{2v} point group (isosceles triangles). Among them, the points at $\phi=\{0; 120°; 240°\}$, which include the three minima, represent the acute triangle geometries. In the case of cyclic-N_3 these geometries exhibit $^2B_1$ symmetry of the ground electronic state. Alternatively, the points at $\phi=\{60°; 180°; 300°\}$, which include the three transition state points, represent the obtuse triangle geometries and exhibit $^2A_2$ symmetry of the ground electronic state. This is visualized in Fig. 1(b) by the symmetry map superimposed with the contour plot of cyclic-N_3 PES. The $^2B_1$ states are symmetric with respect to the permutation of the two nitrogen nuclei that form the base of the isosceles triangle, while the $^2A_2$ states are antisymmetric with respect to this operation. In the APH coordinates, the permutation symmetry corresponds to reflection through the $\phi=n\times 60°$ lines and this is illustrated in Fig. 2, left frame. Note: an observer can encircle the conical intersection by, for example, following the hyperangle ϕ from 0° to 360° and keeping ρ and θ fixed. Alternatively, one may think about encircling the conical intersection by following the minimum energy path that connects all the three minima and the three transition state points. Let us start from

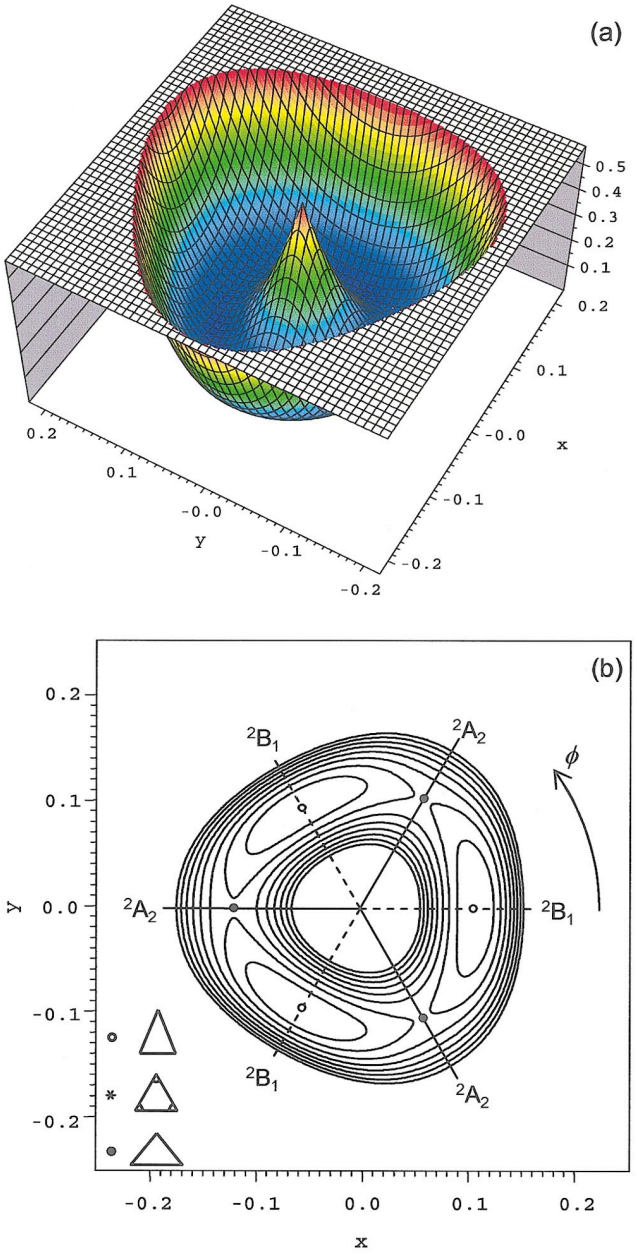

FIG. 1. (Color) A surface plot for the stereographic projection of the cyclic-N_3 PES. The value of the hyperradius is fixed at $\rho=3.4070$ a.u. The conical intersection is seen at ($x=0$, $y=0$). The vertical scale shows the energy in eV. (b) A contour map of (a). Contour lines are given from 0 to 0.16 eV (roughly equal to energy of the BO ground vibrational state) in steps of 0.02 eV. The symbol ○ indicates points of minima and the symbol ● indicates transition state points. A "shape legend" is given in the bottom. Three solid and three dashed lines cross at the point of conical intersection and indicate C_{2v} geometries with $^2A_2$ and $^2B_1$ electronic state symmetries, respectively.

the minimum at $\phi=0$ where the electronic wave function is symmetric ($^2B_1$) and assume, for definiteness, that it is *positive* on both sides of the $\phi=0$ line (see Fig. 2). Going from the minimum at $\phi=0$ to another one at $\phi=120°$ an observer will see that the symmetry of the electronic wave function changes from $^2B_1$ at $\phi=0$ to $^2A_2$ at $\phi=60°$ and back to $^2B_1$ at $\phi=120°$. Since the $^2A_2$ electronic wave function at $\phi=60°$ is antisymmetric it changes sign. As a result, the $^2B_1$ electronic wave function is required to be negative on both sides of $\phi=120°$ line, i.e., it changes sign compared to that at

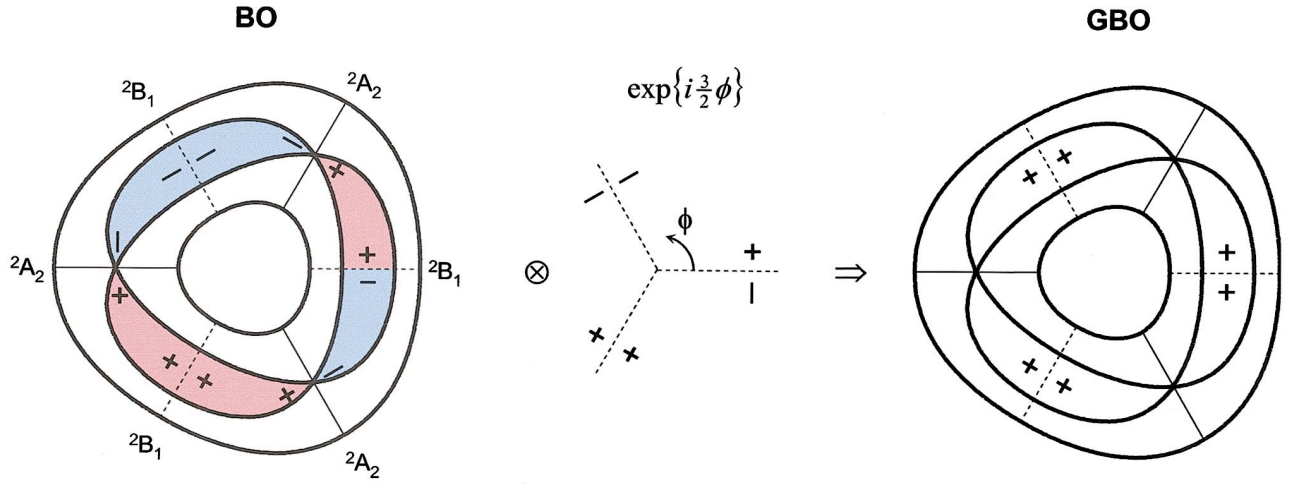

FIG. 2. (Color) Illustration of the sign change in the Born–Oppenheimer electronic wave function. Panels on the left and right sides of the figure represent a contour plot of the cyclic-N_3 PES [as in Fig. 1(b)] but with only two contour lines: one contour line is given at 0.16 eV, which is also the highest energy contour line in Fig. 1(b). It forms two concentric loops of similar shape at the inner and outer parts of the well. The second contour line is given exactly at the energy of the transition state [0.0386 eV, see also Fig. 5(b) in Ref. 7]. This contour line exhibits a Möbius-like shape with the nodes at the transition state points and serves here as a reflection of the electronic wave function symmetries. Namely, the wave function is symmetric across the $^2B_1$ lines and is antisymmetric across the $^2A_2$ lines. This is shown with red and blue colors and is indicated as (+/+) or (+/−) across each C_{2v} symmetry line. However, the BO wave function (left panel) exhibits an abrupt sign change seen as a sharp red-blue boundary at $\phi=0$. This problem is removed by multiplying the real BO wave function by a complex phase factor (middle panel) which exhibits a similar sign change at $\phi=0$. The resultant GBO wave function (right panel) is complex and single-valued everywhere. Note: the signs on the diagrams of the phase factor and the GBO wave function are given only across the $\phi=\{0, 120°, 240°\}$ lines, where they are both real.

$\phi=0$. Going further from $\phi=120°$ to $\phi=240°$ the symmetry again changes from $^2B_1$ to $^2A_2$ at $\phi=180°$ and back to $^2B_1$ and one more sign change occurs as observer reaches $\phi=240°$: the $^2B_1$ electronic wave function is required to be positive on both sides of the $\phi=240°$ line. Further, at $\phi=300°$ the symmetry of the electronic wave function changes one more time to $^2A_2$, and it acquires one more sign change when the observer reaches $\phi=360°$ (returns to $\phi=0$), so that the $^2B_1$ electronic wave function is now required to be *negative* on both sides of the $\phi=360°$ ($\phi=0$) line. Since we started encircling the conical intersection from the assumption that the wave function is positive here, one may say that the electronic wave function is required to be *double valued* at $\phi=0$, which is shown as a sharp red-blue boundary and indicated as $\pm$ in Fig. 2 (left frame). Therefore, as an observer encircles the conical intersection in the APH coordinates, the electronic wave function changes symmetry six times and the sign change of the electronic wave function occurs three times, leading to one net sign change for any complete $0\leqslant\phi\leqslant360°$ loop $s(x)$. It is important to note that the actual electronic structure calculations are performed only in the $0\leqslant\phi\leqslant60°$ range and then the PES data are reflected to cover all values of ϕ. Thus, no problems associated with double-valuedness are encountered in the *electronic structure* calculations. However, the double-valuedness of the electronic wave function must be taken into account in order to obtain the correct *nuclear motion* wave functions (see Sec. III).

III. NUCLEAR SCHRÖDINGER EQUATION

To incorporate the geometric phase effects in the calculations of the vibrational spectra we follow the method proposed by Truhlar and Mead,[9] which was then developed further by Kendrick and Pack[32,33] and successfully applied to accurate calculations of vibrational states.[19,20,34] It requires a generalization of the standard Born–Oppenheimer approximation and we briefly review it here for completeness.

The molecular Schrödinger equation is given by

$$H\Psi_{\text{tot}}=E\Psi_{\text{tot}}, \tag{7}$$

where Ψ_{tot} is the total molecular wave function, H is the total molecular Hamiltonian, and E is the total energy. In the case of triatomic molecules (such as cyclic-N_3) a set of six coordinates is necessary to describe the motion of nuclei relative to the center of mass. Three of these are internal coordinates that depend on the three internuclear distances and are chosen here to be the hyperspherical coordinates $x=(\rho,\theta,\phi)$ introduced in the preceding section. The remaining three nuclear coordinates are the rotational coordinates and are taken as the usual Euler angles $\hat{x}=(\alpha,\beta,\gamma)$ that specify orientation of the body frame relative to the space frame. The whole set of six nuclear coordinates is denoted as $\mathbf{x}=(x,\hat{x})$.

One can separate the center-of-mass motion and express H in the space frame as

$$H\equiv-\frac{\hbar^2}{2\mu}\nabla^2+h(\mathbf{r};x), \tag{8}$$

where the Laplacian is six dimensional with respect to the six nuclear coordinates $\mathbf{x}=(x,\hat{x})$, μ is the three-body reduced mass: $\mu\equiv\sqrt{m_1m_2m_3/(m_1+m_2+m_3)}$, and $h(\mathbf{r};x)$ is the electronic Hamiltonian that depends only parametrically on internal nuclear coordinates x, $\mathbf{r}$ denotes all of the electronic coordinates.

In the present treatment we neglect all electronic angular momentum (spin and orbital) so that the space-frame elec-

tronic eigenfunctions φ_n depend parametrically on the internal nuclear coordinates x and can be chosen real orthogonal with real eigenvalues V_n. As usual, we assume that the electronic part of the problem

$$h(\mathbf{r};x)\varphi_n(\mathbf{r};x)=V_n(x)\varphi_n(\mathbf{r};x) \tag{9}$$

has been accurately solved. Thus, the total molecular wave function can be expanded in terms of a complete set of electronic eigenfunctions:

$$\Psi_{\text{tot}}=\sum_{n=0}^{\infty}\psi_n(\mathbf{x})\varphi_n(\mathbf{r};x), \tag{10}$$

where the expansion coefficients $\psi_n(\mathbf{x})$ are the six-dimensional nuclear motion wave functions. For low vibrational energies one can often neglect the coupling to excited electronic states and truncate the sum in Eq. (10) to only one term

$$\Psi_{\text{tot}}\approx\psi_0(\mathbf{x})\varphi_0(\mathbf{r};x), \tag{11}$$

where $n=0$ corresponds to the ground adiabatic electronic state. For higher vibrational energies more terms in the sum over n must be included and a more general treatment is necessary.[43,44] Thus, in the case of cyclic-N_3, for the vibrational states with energies close to the conical intersection, it may be necessary to include the first excited doublet electronic state in the calculations. We plan to explore this topic in future work. In the present work, we restrict our consideration to the ground doublet electronic state of cyclic-N_3 and drop the subscripts in Eq. (11) assuming that it describes the ground adiabatic electronic state.

Finally, we substitute the expansion (11) into the Schrödinger equation (7) and obtain the standard Born–Oppenheimer (BO) equation

$$\text{BO:}\quad\left\{-\frac{\hbar^2}{2\mu}\nabla^2+V(x)\right\}\psi(\mathbf{x})=E\psi(\mathbf{x}). \tag{12}$$

Deriving this equation we used the property $\langle\varphi(x)|\nabla|\varphi(x)\rangle=0$, which is straightforward to prove by differentiating the normality condition $\langle\varphi(x)|\varphi(x)\rangle=1$ and taking into account that $|\varphi(x)\rangle$ is real. Solutions $\psi(\mathbf{x})$ of the BO nuclear motion equation (12) are real and single valued.

Now we recall that the real ground state electronic eigenfunction $\varphi(\mathbf{r};x)$ is double valued. It changes sign whenever the nuclear motion $s(x)$ encircles the conical intersection between the ground and the first excited electronic states. In the case of cyclic-N_3 the actual conical intersection occurs at high energies ($\sim$4600 cm^{-1}) but it is important to realize that the sign change occurs for much lower energies. The vibrational energy only needs to be high enough to allow the nuclei to go over the pseudorotation barrier ($\sim$311 cm^{-1}) so that the nuclear motion $s(x)$ can encircle the intersection. In our previous paper,[7] we predicted that the energy of the BO ground vibrational state in cyclic-N_3 is $\sim$1312 cm^{-1} (i.e., well above the pseudorotation barrier). Thus, significant geometric phase effects should occur for all vibrational states of cyclic-N_3 without exceptions, even for its ground vibrational state. In order for the total wave function Ψ_{tot} of Eq. (7) to remain single valued and maintain the correct permutation symmetry for all nuclear configurations, the nuclear motion wave function $\psi(\mathbf{x})$ must also change sign [i.e., it should also be double valued such as $\varphi(\mathbf{r};x)$]. However, in the standard BO approach there is no built-in mechanism to ensure that the nuclear motion wave function in Eq. (12) changes sign as the nuclear motion $s(x)$ encircles the conical intersection.

To overcome this inconsistency, we follow the method of Mead and Truhlar[9] and multiply the real adiabatic electronic wave function by a complex phase factor

$$\varphi^G(\mathbf{r};x)=\varphi(\mathbf{r};x)\cdot\exp\left\{i\frac{\ell}{2}\eta(x)\right\}, \tag{13}$$

where ℓ is an *odd* integer and $\eta(x)$ is an angle function that changes by 2π for any nuclear motion $s(x)$ that encircles the conical intersection. The role of the phase factor in Eq. (13) is to cancel the sign change in the *real double-valued* $\varphi(\mathbf{r};x)$ giving rise to a *complex single-valued* electronic wave function $\varphi^G(\mathbf{r};x)$. For symmetry reasons, the most convenient value of the gauge parameter for the description of triatomic molecules is $\ell=3$. Figure 2 illustrates how the $\exp\{i3/2\eta(x)\}$ transformation (in the middle of figure) cancels the sign change in the real double valued $\varphi(\mathbf{r};x)$ function (left frame) and produces the complex single-valued $\varphi^G(\mathbf{r};x)$ function (right frame).

Using the $\varphi^G(\mathbf{r};x)$ wave functions (13) for the expansion of Ψ_{tot} and substituting the result into the Schrödinger equation (7) we obtain [instead of Eq. (12)] the generalized (GBO) equation for the nuclear motion

$$\text{GBO:}\quad\left\{\frac{\hbar^2}{2\mu}[-i\nabla-\mathbf{A}(x)]^2+V(x)\right\}\psi^G(\mathbf{x})=E\psi^G(\mathbf{x}), \tag{14}$$

where $\mathbf{A}(x)$ is called the vector potential defined as

$$\mathbf{A}(x)\equiv i\langle\varphi^G(x)|\nabla|\varphi^G(x)\rangle. \tag{15}$$

The most important point here is that the solutions $\psi^G(\mathbf{x})$ of the nuclear motion equation (14) are now complex single valued, so that no sign inconsistencies occur in the GBO formulation.

Furthermore, by applying the appropriate phase factors and projection operators to the complex single-valued solutions $\psi^G(\mathbf{x})$, it is possible to obtain the real double-valued solutions with the correct permutation symmetry. Cyclic-N_3 contains three identical nuclei so that the symmetry of its vibrational eigenstates can be classified using the irreducible representations of the permutation group S_3. This group has two nondegenerate irreducible representations, A_1 and A_2, and one doubly degenerate irreducible representation E. The A_1 (A_2) vibrational eigenstates are symmetric (antisymmetric) with respect to an exchange of any two of the three nuclei. The solutions of A_1 and A_2 symmetry can be obtained via[9,20]

$$\psi_{A_1}=[(1+P_{123}+P_{321})\psi^G]\cdot\exp\left\{i\frac{\ell}{2}\eta(x)\right\}+[(P_{12}+P_{23}+P_{31})\psi^G]\cdot\exp\left\{-i\frac{\ell}{2}\eta(x)\right\}, \quad (16)$$

$$\psi_{A_2}=-i\left([(1+P_{123}+P_{321})\psi^G]\cdot\exp\left\{i\frac{\ell}{2}\eta(x)\right\}-[(P_{12}+P_{23}+P_{31})\psi^G]\cdot\exp\left\{-i\frac{\ell}{2}\eta(x)\right\}\right). \quad (17)$$

The real double-valued solutions of E symmetry can be obtained in three steps.[20] In the first step, the E symmetry projection operator is applied to the complex solutions to obtain symmetrized complex solutions via

$$\tilde{\psi}^G=[(2-P_{123}-P_{321})\psi^G]\cdot\exp\left\{i\frac{\ell}{2}\eta(x)\right\}. \quad (18)$$

In the second step, each pair of the degenerate symmetrized complex wave functions $\tilde{\psi}^G$ is used to construct a pair of real double-valued degenerate wave functions by taking the real part of one of the degenerate symmetrized complex wave functions and the imaginary part of the other. In the third step, the set of these real double-valued wave functions is orthogonalized using the Schmidt orthogonalization procedure to obtain solutions ψ_E. The permutation symmetries of the ψ_{A_1}, ψ_{A_2}, and ψ_E will be further discussed in Sec. VI and their relevance to the cancelation of the sign change will be demonstrated.

An expression for the GBO kinetic energy operator for nonzero total angular momentum in the hyperspherical coordinates has been derived in Ref. 32:

$$\frac{\hbar^2}{2\mu}[-i\nabla-\mathbf{A}(x)]^2=-\frac{\hbar^2}{2\mu\rho^5}\frac{\partial}{\partial\rho}\rho^5\frac{\partial}{\partial\rho}-\frac{4\hbar^2}{2\mu\rho^2}\left[\frac{1}{\sin 2\theta}\frac{\partial}{\partial\theta}\sin 2\theta\frac{\partial}{\partial\theta}+\frac{1}{\sin^2\theta}\frac{\partial^2}{\partial\phi^2}\right]+\frac{1}{\mu\rho^2}\left[\frac{J_x^2}{(1-\sin\theta)}+\frac{J_y^2}{(1+\sin\theta)}+\frac{J_z^2}{2\sin^2\theta}\right]+i\frac{\hbar^2}{2\mu}\left[\frac{5}{\rho}A_\rho+\frac{\partial A_\rho}{\partial\rho}+\frac{8\cot 2\theta}{\rho^2}A_\theta+\frac{4}{\rho^2}\frac{\partial A_\theta}{\partial\theta}+\frac{4}{\rho^2\sin^2\theta}\frac{\partial A_\phi}{\partial\phi}+2A_\rho\frac{\partial}{\partial\rho}+\frac{8}{\rho^2}A_\theta\frac{\partial}{\partial\theta}+\frac{8}{\rho^2\sin^2\theta}A_\phi\frac{\partial}{\partial\phi}\right]+\frac{\hbar^2}{2\mu}\left[A_\rho^2+\frac{4}{\rho^2}A_\theta^2+\frac{4}{\rho^2\sin^2\theta}A_\phi^2\right]+\frac{4\hbar\cos\theta}{2\mu\rho^2\sin^2\theta}J_z\left[\frac{1}{i}\frac{\partial}{\partial\phi}-A_\phi\right]. \quad (19)$$

Using Eq. (13) in Eq. (15) we obtain for the three components of the vector potential in the hyperspherical coordinates

$$A_\rho(x)=-\frac{\ell}{2}\frac{\partial\eta(x)}{\partial\rho}, \quad (20a)$$

$$A_\theta(x)=-\frac{\ell}{2}\frac{\partial\eta(x)}{\partial\theta}, \quad (20b)$$

$$A_\phi(x)=-\frac{\ell}{2}\frac{\partial\eta(x)}{\partial\phi}. \quad (20c)$$

The explicit functional form of $\eta(x)$ is somewhat arbitrary; the only requirement is that $\eta(x)$ changes by 2π for any path that encircles the conical intersection. The general expression for $\eta(x)=\eta(\rho,\theta,\phi)$ in the hyperspherical coordinates (derived in Appendix B of Ref. 32) is especially simple in the case of the D_{3h} conical intersection

$$\eta=\phi. \quad (21)$$

Therefore, for the D_{3h} conical intersection we obtain from Eqs. (20a)–(20c)

$$A_\rho(x)=0, \quad (22a)$$

$$A_\theta(x)=0, \quad (22b)$$

$$A_\phi(x)=-\frac{\ell}{2}. \quad (22c)$$

This vector potential has only one nonzero component A_ϕ, so that the kinetic energy operator (19) simplifies significantly (for $J=0$):

$$\frac{\hbar^2}{2\mu}[-i\nabla-\mathbf{A}(x)]^2=-\frac{\hbar^2}{2\mu\rho^5}\frac{\partial}{\partial\rho}\rho^5\frac{\partial}{\partial\rho}-\frac{4\hbar^2}{2\mu\rho^2}\frac{1}{\sin 2\theta}\frac{\partial}{\partial\theta}\sin 2\theta\frac{\partial}{\partial\theta}-\frac{4\hbar^2}{2\mu\rho^2}\frac{1}{\sin^2\theta}\left(\frac{\partial^2}{\partial\phi^2}-2iA_\phi\frac{\partial}{\partial\phi}-A_\phi^2\right). \quad (23)$$

Finally, the kinetic energy operator can be presented in the following compact form:

$$\frac{\hbar^2}{2\mu}[-i\nabla-\mathbf{A}(x)]^2=-\frac{\hbar^2}{2\mu\rho^5}\frac{\partial}{\partial\rho}\rho^5\frac{\partial}{\partial\rho}-\frac{4\hbar^2}{2\mu\rho^2}\frac{1}{\sin 2\theta}\frac{\partial}{\partial\theta}\sin 2\theta\frac{\partial}{\partial\theta}-\frac{4\hbar^2}{2\mu\rho^2}\frac{1}{\sin^2\theta}\left(\frac{\partial}{\partial\phi}+i\frac{\ell}{2}\right)^2. \quad (24)$$

For future reference we would like to mention that the expression (24) contains four singular terms. Two of them,

$$\frac{^1 1}{\sin 2\theta} \to \infty \quad \left(\theta \to 0 \quad \text{and} \quad \theta \to \frac{\pi}{2}\right), \tag{25}$$

$$\frac{1}{\sin^2 \theta} \frac{\partial^2}{\partial \phi^2} \to \infty \quad (\theta \to 0), \tag{26}$$

are well known as Eckart singularities and will be treated in both BO and GBO calculations by the appropriate choice of the basis set.[41] The other two are relevant to the vector potential

$$A_\phi \frac{1}{\sin^2 \theta} \frac{\partial}{\partial \phi} \to \infty \quad (\theta \to 0), \tag{27}$$

$$A_\phi^2 \frac{1}{\sin^2 \theta} \to \infty \quad (\theta \to 0). \tag{28}$$

They appear only in the GBO treatment and occur at the point of the conical intersection.

IV. NUMERICAL TECHNIQUES

The potential energy surface $V(\rho, \theta, \phi)$ strongly couples internal degrees of freedom so that the Schrödinger equation, either Eq. (12) or Eq. (14), is nonseparable and cannot be solved by analytical decoupling. Therefore, we decouple the radial and angular coordinates numerically using the sector adiabatic approach.[40] In this approach, the full dimensional Schrödinger equation is solved in two steps. In the first step the hyperradius ρ is partitioned into a large number of sectors (intervals) and the angular (θ,ϕ) part of the equation is solved numerically for each sector with ρ (as a parameter) fixed at the center of each sector. The potential coupling matrices and overlap matrices between the neighboring (adjacent) sectors are also computed at this step. In the second step, a set of one-dimensional coupled-channel (CC) equations is obtained for the hyperradial ρ coordinate[40] and is solved using a numerical propagation technique. In this way, the accurate full dimensional solutions of the Schrödinger equation are obtained using the exact Hamiltonian and including all couplings.

The parallel computer code of Kendrick, applied previously to calculate bound states in the HO_2 (Ref. 34) and Na_3 molecules,[19,20] was used in this work. This code employs an efficient hybrid FBR/DVR (Ref. 32) algorithm to solve the angular (θ,ϕ) part of the problem and uses the Numerov method[45] for solution of the coupled-channel equations in ρ. The range of ρ=[3.185 a.u.; 3.925 a.u.] was partitioned onto 149 sectors using a constant step size of $\Delta\rho$=0.005 a.u. The dimension of the DVR in θ based on Jacobi polynomials was 104, which corresponds to the number of Gauss–Legendre quadrature points in $\tilde{\theta} = \pi - 2\theta$.[32] The FBR in ϕ uses the complex exponential functions[32] and its basis set size was 201. The cutoff value for the sequential diagonalization truncation algorithm[32] was set at 10 eV. The coupled-channel equations in ρ contained 35 channels for A_1 and A_2 symmetry solutions and 140 channels (70 doubly degenerate channels) for E symmetry solutions.

The overall accuracy of our results with respect to the positions of $\rho_{\min}$ and $\rho_{\max}$, number of sectors in ρ, energy cutoff value, 2D basis set size in θ and ϕ, number of coupled channels in ρ and convergence of the Numerov bisections is better than 1 cm^{-1}.

V. STANDARD BO RESULTS

Although the results obtained by solving the standard Born–Oppenheimer equation (12) are, formally, incorrect, they are important for several reasons: First of all, we want to compare them with the correct results obtained by solving the generalized Born–Oppenheimer equation (14) in order to quantify the value of the geometric phase effects in the vibrational eigenvalues. This will allow us to make a conclusion about the importance of such effects in the case of cyclic-N_3 and usefulness (or uselessness) of the standard BO approach where these effects are neglected. Second, we want to visualize the vibrational eigenfunctions obtained from both the standard and the generalized BO equations in order to demonstrate qualitatively how the vector potential A_ϕ in Eq. (14) affects the node structure of the vibrational wave functions. This will help our intuitive understanding of the geometric phase.

In the Tables I, II, and III we give eigenvalues of the symmetries A_1, A_2, and E, respectively, computed for cyclic-N_3 using the standard BO approach. The energy range extends from the ground vibrational state up to the energy of the conical intersection. In some cases, several states above the conical intersection are also given for the reason that will become clear in the following section. The vibrational wave functions for all these states are plotted in Figs. 3, 4, and 5 for symmetries A_1, A_2, and E, respectively, using the 3D isosurfaces in the hyperspherical coordinates. Using these 3D plots we have assigned all the states in Tables I–III in terms of the normal vibration mode quantum numbers and those assignments are given in the third column of each Table as (v_1,v_2,v_3)=(symmetric stretch, bend, asymmetric stretch). Although, the hyperspherical coordinates are different from the normal mode coordinates, it is very useful to remember that a displacement along the hyperradius ρ corresponds to symmetric stretch of the cyclic-N_3 triatomic, while displacements along the hyperangles θ and ϕ correspond to the bend and asymmetric stretch respectively. A schematic is given in Fig. 6 to facilitate the normal mode analysis of the wave functions in Figs. 3–5 (and in Figs. 7–9 below). Based on these 3D plots the normal mode assignments are straightforward for almost all states except a few, where the structure of the vibrational wave function is complicated by the intermode coupling and/or interaction with another state. In such cases assignments based on the energy quanta is not very helpful either, so that the visual representation is still useful, though assignment is not immediately obvious.

The lowest energy state is the ground vibrational state of A_1 symmetry assigned as (0,0,0). The A_1 symmetry states are restricted to be symmetric with respect to reflection through the ϕ={0; 120°; 240°} planes, so that the 3D wave function of the (0,0,0) A_1 state is basically a torus (see Fig. 3, frame no. 1) that encircles the conical intersection line (i.e., the ρ axis). The internal circumference of such a torus follows the hyperangle ϕ with (roughly) constant θ and ρ. This shape mimics the shape of the PES shown in Fig. 6(a) of

TABLE I. BO and GBO energies and assignments of the vibrational states of A_1 symmetry in cyclic-N_3.

State no.	BO energies (cm^{-1})	BO assignments (v_1,v_2,v_3)	GBO gauge error (cm^{-1})	GBO energies (cm^{-1})	GBO assignments; BO state no.	Geometric phase effect (GBO-BO)(cm^{-1})
1	1310.65	(0,0,0)	0.144	1401.22	(0,0,0); 1	90.56
2	1810.07	(0,0,2)	0.002	2262.31	(0,1,0); 3	133.35
3	2128.96	(0,1,0)	1.480	2269.93	(0,0,2); 2	459.86
4	2687.09	(0,1,2)	0.112	3003.67	(1,0,0); 6	146.82
5	2827.31	(0,0,4)	−0.002	3123.31	(0,2,0); 7	172.87
6	2856.85	(1,0,0)	3.309	3175.60	(0,1,2); 4	488.51
7	2950.44	(0,2,0)	4.215	3435.95	(0,0,4); 5	608.65
8	3402.15	(1,0,2)	0.029	3871.90	(1,1,0);10	223.50
9	3559.65	(0,2,2)	1.674	3928.34	(1,0,2); 8	526.19
10	3648.40	(1,1,0)	16.846	3984.73	(0,3,0);12	204.55
11	3741.51	(0,1,4)	0.073	4071.50	(0,2,2); 9	511.85
12	3780.18	(0,3,0)	5.820	4349.79	(0,1,4);11	608.28
13	4078.57	(0,0,6)	−0.015	4601.27	(2,0,0);15	236.46
14	4292.20	(1,1,2)	0.185			
15	4364.81	(2,0,0)	19.615			
16	4446.42	(2,0,2)	1.786			
17	4468.27	(1,2,0)	26.709			
18	4510.59	(1,0,4)	0.031			

Ref. 7. There are not any nodes in the wave function of the ground state. The first excited state of A_1 symmetry is (0,0,2). It exhibits two nodes along ϕ coordinate across each well (see the well at $-60° \leqslant \phi \leqslant 60°$, for example). Due to symmetry there are six such nodes in the whole range of $0 \leqslant \phi \leqslant 360°$. This corresponds to two quanta of asymmetric stretch. The next excited state is (0,1,0) and its wave function exhibits one node along the θ coordinate (it basically consists of two tori), which corresponds to one quantum of bend. The next excited state is the combination state (0,1,2) and its wave function structure reflects a superposition of these three quanta. Higher in energy we see the overtone state (0,0,4), which exhibits four nodes along the ϕ coordinate in the range $-60° \leqslant \phi \leqslant 60°$ (12 nodes in the whole range of ϕ). The next state is an excited symmetric stretch state (1,0,0), which exhibits one node along ρ. We let the readers look through the remaining frames of Fig. 3 and follow the assignments. The assignments of states 15, 16, and 17 were more difficult and required plotting several isosurfaces of these wave functions at different values of the probability amplitude.

For future reference we note that, as clearly seen in Fig. 3, the BO wave functions for several vibrational eigenstates exhibit nonzero probability in the center, along the ρ axis. These are the states 6, 7, 10, 12, 15, and 17. Energies of all these states are below the energy of the conical intersection. However, due to quantum mechanical tunneling, the wave functions of these states reach the point of the conical intersection (i.e., they do not vanish at $\theta=0$). One can say that such vibrational states tunnel through the conical intersection. We will come back to discussion of the consequences of this effect in the following section.

The states of A_2 symmetry are restricted to be antisymmetric with respect to reflection through the $\phi=\{0; 120°; 240°\}$ planes. Therefore, the ground vibrational state of A_2 symmetry (see Fig. 4, frame no. 1) exhibits nodes there.

TABLE II. BO and GBO energies and assignments of the vibrational states of A_2 symmetry in cyclic-N_3.

State no.	BO energies (cm^{-1})	BO assignments (v_1,v_2,v_3)	GBO gauge error (cm^{-1})	GBO energies (cm^{-1})	GBO assignments; BO state	Geometric phase effect (GBO-BO)(cm^{-1})
1	1787.52	(0,0,1)	−0.002	1501.68	(0,0,1); 1	−285.84
2	2673.59	(0,1,1)	0.002	2272.38	(0,0,3); 3	−554.02
3	2826.40	(0,0,3)	−0.010	2339.15	(0,1,1); 2	−334.44
4	3399.24	(1,0,1)	−0.009	3038.19	(1,0,1); 4	−361.05
5	3552.35	(0,2,1)	0.022	3176.02	(0,2,1); 5	−376.33
6	3739.59	(0,1,3)	−0.023	3183.82	(0,1,3); 6	−555.77
7	4078.39	(0,0,5)	−0.031	3436.32	(0,0,5); 7	−642.07
8	4306.40	(1,1,1)	0.002	3869.42	(1,1,1); 8	−436.98
9	4425.68	(0,3,1)	0.072	3937.11	(1,0,3);10	−572.77
10	4509.88	(1,0,3)	−0.029	4017.89	(0,3,1); 9	−407.79
11	4645.23	(0,2,3)	−0.048	4078.60	(0,2,3);11	−566.63
12	4989.68	(0,1,5)	−0.058	4350.35	(0,1,5);12	−639.33
13	5011.66	(2,0,1)	−0.023	4576.80	(2,0,1);13	−434.86

TABLE III. BO and GBO energies and assignments of the vibrational states of E symmetry in cyclic-N_3.

State no.	BO energies (cm^{-1})	BO assignments (v_1,v_2,v_3)	GBO gauge error (cm^{-1})	GBO energies (cm^{-1})	GBO assignments; BO state no.	Geometric phase effect (GBO-BO)(cm^{-1})
1	1364.95	(0,0,0)	0.020	1325.67	(0,0,0); 1	−39.28
2	1560.68	(0,0,1)	−0.414	1668.88	(0,0,1); 2	108.20
3	2101.70	(0,0,2)	−0.078	1944.56	(0,0,2); 3	−157.14
4	2207.14	(0,1,0)	−0.119	2151.49	(0,1,0); 4	−55.65
5	2417.35	(0,1,1)	−0.059	2540.71	(0,1,1); 5	123.37
6	2448.36	(0,0,3)	0.572	2634.44	(0,0,3); 6	186.08
7	2931.49	(1,0,0)	−0.374	2828.28	(0,1,2); 8	−178.33
8	3006.61	(0,1,2)	−0.143	2888.24	(1,0,0); 7	−43.25
9	3048.65	(0,2,0)	0.054	2981.24	(0,0,4);11	−67.41
10	3132.04	(1,0,1)	−0.492	3025.22	(0,2,0); 9	−203.31
11	3228.53	(0,0,4)	0.452	3257.48	(1,0,1);10	125.43
12	3274.71	(0,2,1)	−0.059	3409.79	(0,2,1);12	135.08
13	3358.79	(0,1,3)	0.276	3546.25	(0,1,3);13	187.46
14	3647.56	(0,0,5)	0.000	3557.27	(1,0,2);15	−163.34
15	3720.61	(1,0,2)	0.231	3690.31	(1,1,0);16	−101.98
16	3792.29	(1,1,0)	−0.394	3735.22	(0,2,2);18	−166.66
17	3885.33	(0,3,0)	0.098	3816.54	(0,3,0);17	−68.79
18	3901.87	(0,2,2)	−0.236	3861.90	(0,0,5);14	214.34
19	4008.01	(1,1,1)	0.315	3939.78	(0,1,4);22	−203.31
20	4112.77	(1,0,3)	−0.040	4148.60	(1,1,1);19	140.60
21	4133.44	(0,3,1)	0.040	4276.10	(0,3,1);21	142.66
22	4143.09	(0,1,4)	−0.098	4297.47	(0,0,6);25	−220.54
23	4258.87	(0,2,3)	−0.197	4309.19	(1,0,3);20	196.42
24	4491.82	(2,0,0)	−0.177	4419.59	(2,0,0);24	−72.24
25	4518.01	(0,0,6)	−0.295	4449.09	(0,2,3);23	190.22

Since the wave function is real, the nodes are also required at the transition states (six nodes total in $0 \leqslant \phi \leqslant 360°$, see Fig. 10 below, lower left panel). Because there is only one node across each well (see the well at $-60° \leqslant \phi \leqslant 60°$, for example) such a 3D wave function corresponds to one quantum of asymmetric stretch, so that the lowest energy state of A_2 symmetry is assigned as (0,0,1). The wave function of this state looks very similar to the wave function of (0,0,2) A_1 symmetry state (Fig. 3, frame no. 2) except that it is twisted by $\phi = 30°$ around the ρ axis. Thus, the nodes of the A_1 symmetry state coincide with the maxima of the A_2 symmetry state, and vice versa. Not only the eigenfunctions of these states look very similar, but also their eigenvalues differ only by $\sim 23\ cm^{-1}$. Such a close similarity exists between several other states of A_1 and A_2 symmetries and we let readers find the relevant frames in Figs. 3 and 4 (keep in mind that all A_2 symmetry states are required to have at least one quantum of the asymmetric stretch) and check that the corresponding energy shifts, calculated from Tables I and II, are relatively small. This occurs because of the very low value of the pseudorotation barrier in cyclic-N_3. The nodes of the wave function for the (0,0,2) state of A_1 symmetry are at $\phi = 30° + n \times 60°$, where n is an integer (i.e., they all are in the middle between the minima and the transition state points). The nodes of wave function for the (0,0,1) state of A_2 symmetry are at $\phi = n \times 60°$ [i.e., three of them are at the minima and the other three are at the transition state points, see Fig. 1(b)]. In the hypothetical example of zero energy transition states (no pseudorotation barrier), these solutions of A_1 and A_2 symmetries will become degenerate. However, in the real cyclic-N_3, the barrier is not zero but it is still small compared to the energy of the vibrational states. Thus, the energy difference between the states of A_1 and A_2 symmetries is also small.

The wave functions of the E symmetry states are given in Fig. 5, where each frame contains two wave functions of the degenerate E states. The nodal structures of the wave functions within each pair are similar, except that one of them is twisted by $\phi = 45°$ around the ρ axis. The wave functions of E symmetry states contain fewer nodes in ϕ than the wave functions of A_1 and A_2 symmetry states. For example, the (0,0,3) E symmetry state exhibits ten nodes along ϕ coordinate, while the (0,0,3) state of A_2 symmetry exhibits 12 nodes along ϕ. Again, the assignments of the normal mode quantum numbers are straightforward for most of the states, except for the states 16, 17, and 18, and we let the readers follow the assignments in Fig. 5.

VI. GENERALIZED BO RESULTS

It is instructive to perform several independent sets of generalized BO calculations with different values of the gauge parameter ℓ. Calculations with $\ell = 0$ must be identical to the *standard* BO approach and we have performed such $\ell = 0$ calculations only in order to check that this is indeed the case. Calculations performed with $\ell = 3$ are the actual GBO calculations and these results are presented further in this section. They will be compared to the standard BO calculations (reported in the preceding section) in order to quantify the magnitude of the geometric phase effect for every state. Calculations with $\ell = 6$ should, at least in principle, be equivalent to those with $\ell = 0$ and the standard BO results, so

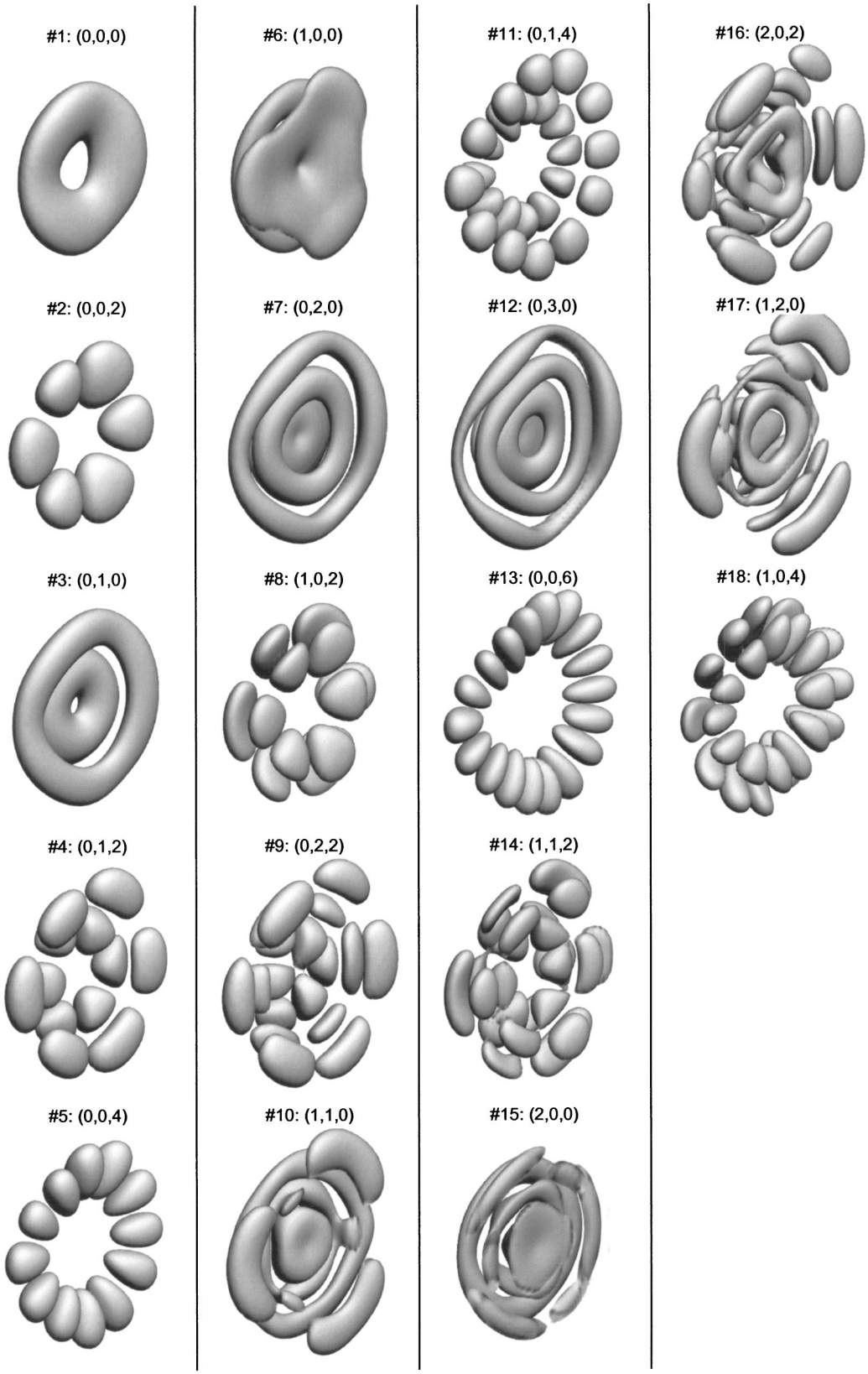

FIG. 3. Three-dimensional wave functions for BO vibrational eigenstates of A_1 symmetry in cyclic-N_3. Isosurfaces of the probability amplitude are plotted at the value of 0.05 using the hyperspherical coordinates. A schematic of the hyperspherical coordinates is given in Fig. 6 to facilitate analysis of the nodal structure of these wave functions. Assignments in terms of the normal mode quantum numbers are given on top of each wave function. See text for discussion.

that any deviations are indicatives of some numerical problems in the $\ell \neq 0$ calculations (convergence and other issues discussed below). This is very helpful, since the differences between the $\ell=0$ and $\ell=6$ calculations can be used as the upper bounds of numerical errors associated with incorporation of the vector potential into the Schrödinger equation (14). Therefore, we performed the $\ell=6$ calculations as well, computed the differences with $\ell=0$ results and reported them

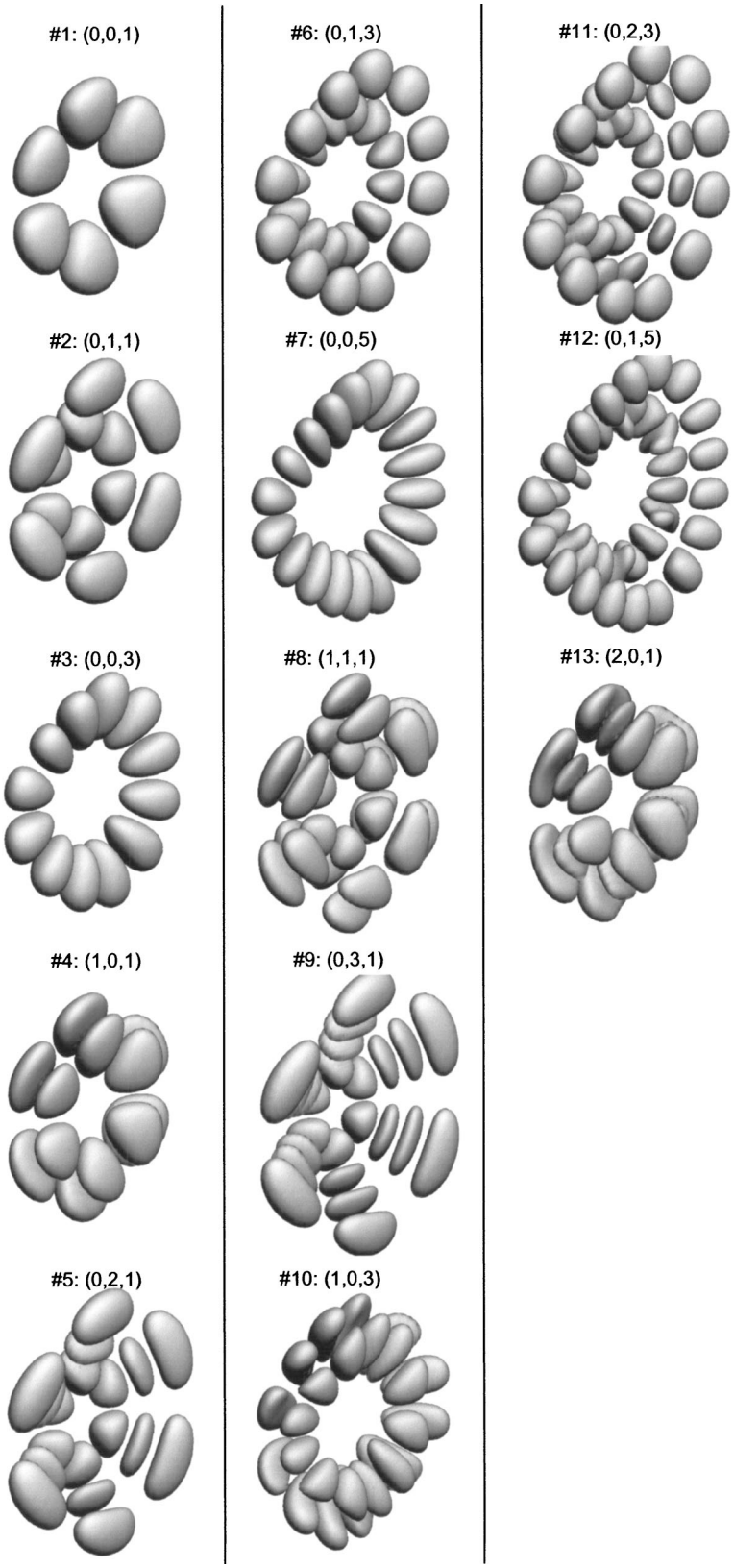

FIG. 4. Three-dimensional wave functions for BO vibrational eigenstates of A_2 symmetry in cyclic-N_3. As discussed in the text, the states of this symmetry are restricted to have at least one quantum of asymmetric stretch, so that the spectrum starts with the (0,0,1) state.

further in this section as the "errors" of the GBO calculations. Calculations with $\ell=9$ should again be identical to $\ell=3$ and we have found that they are indeed practically identical, so that there is no reason to perform calculations with any $\ell>9$. To summarize, we have performed four independent sets of the generalized BO calculations with $\ell=0$, 3, 6, and 9.

In the fifth column of Tables I, II and III we give eigenvalues of the symmetries A_1, A_2, and E, respectively, computed for cyclic-N_3 using the GBO approach. The real

double-valued vibrational wave functions ψ_{A_1}, ψ_{A_2}, and ψ_E for all these eigenstates are plotted in Figs. 7, 8, and 9, respectively, using 3D isosurfaces in the hyperspherical coordinates. Prior to analyzing all the wave functions in Figs. 7–9 let us understand how the geometric phase changes the nodal structure of the vibrational wave functions. Figure 10 shows 2D slices of the wave functions for the (0,0,0) state of A_1 symmetry and the (0,0,1) state of A_2 symmetry, which are the lower energy vibrational states of these symmetries. In this figure the color is used to show the sign of each part of the vibrational wave function—information that is not seen in Figs. 3–5 and 7–9, where only the $|\psi|^2$ is presented. Two slices on the left are from the BO calculations, while two slices on the right are from the GBO calculations. The BO wave functions are single valued everywhere. However, the GBO wave functions are double valued at $\phi=0$ [i.e., they exhibit the sign change when the nuclear motion $s(x)$ encircles the conical intersection]. Indeed, the GBO wave func-

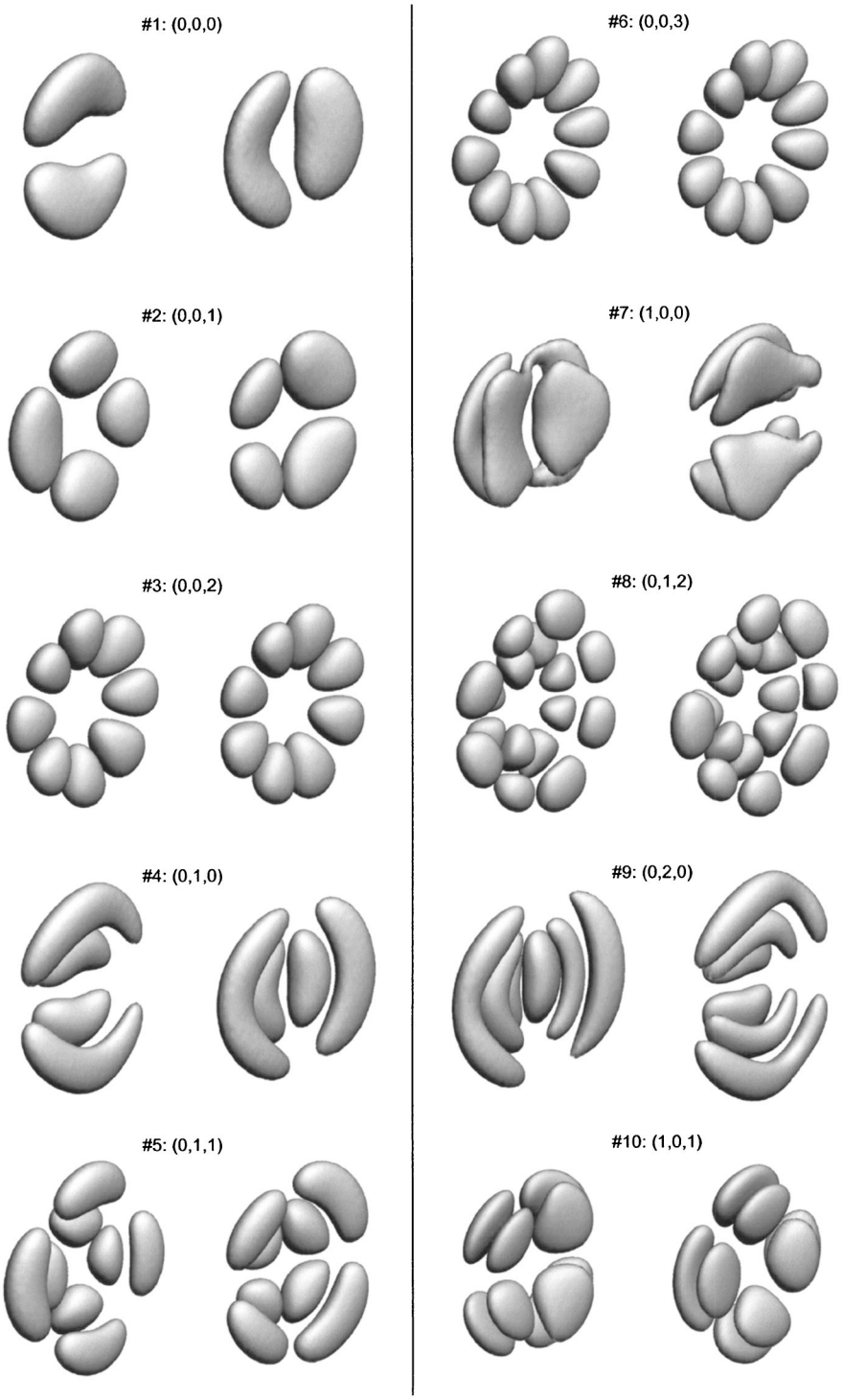

FIG. 5. Three-dimensional wave functions for BO vibrational eigenstates of E symmetry in cyclic-N_3. Each panel contains two wave functions for two degenerate states of E symmetry.

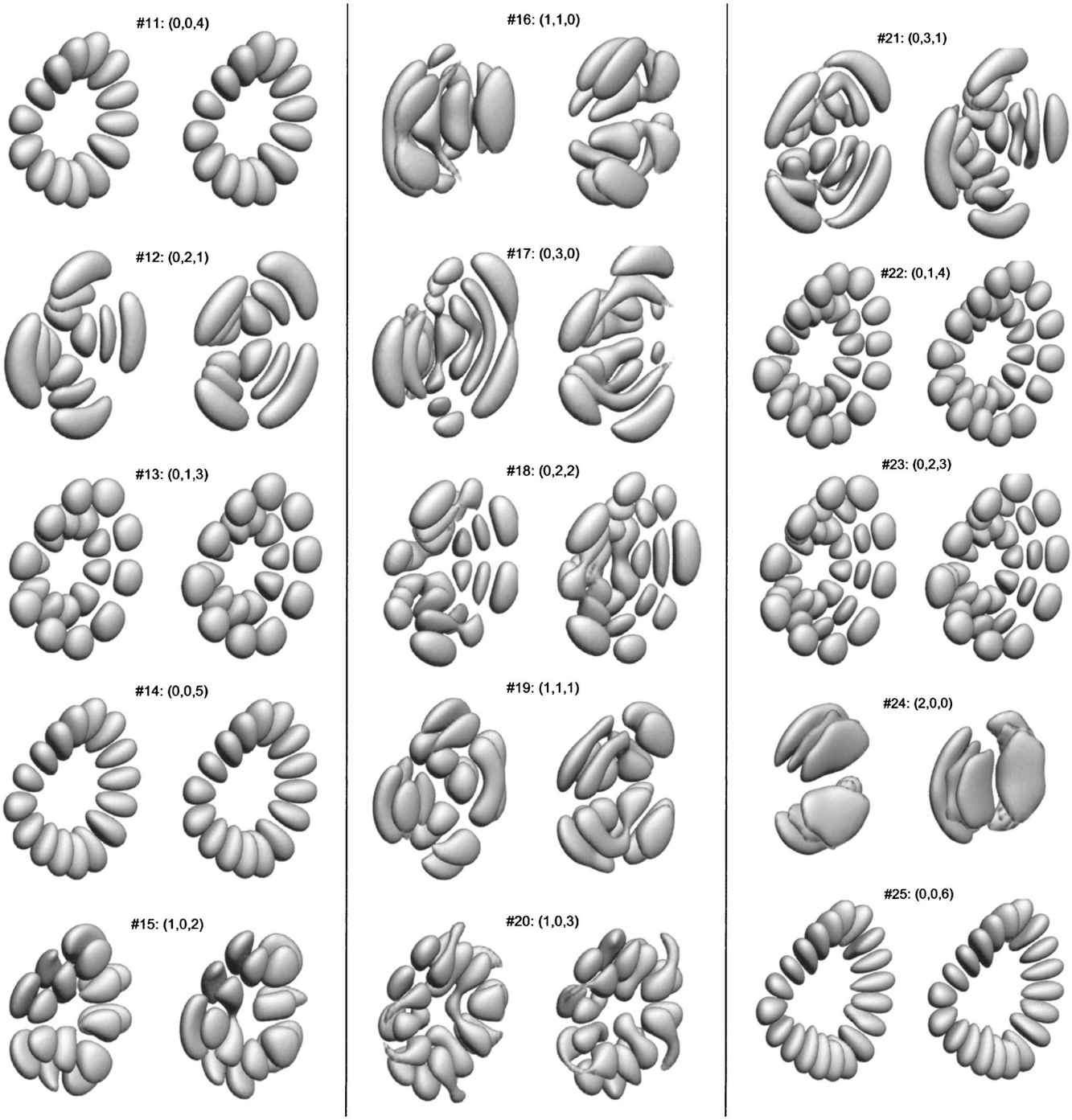

FIG. 5. (*Continued.*)

tion of A_1 symmetry changes sign at $\phi=0$, whereas the BO one is symmetric. Similarly, the GBO wave function of A_2 symmetry is positive across the node at $\phi=0$, whereas the BO one changes sign. Such a behavior is analogous to the behavior of the BO electronic wave function illustrated in the left frame of Fig. 2. By construction, the product of the real double-valued vibrational wave functions with the real double-valued electronic wave function results in single-valued total wave functions which exhibit the correct permutation symmetry everywhere. To see that this is indeed achieved in our GBO results, take each GBO vibrational wave function (A_1 or A_2) in Fig. 10 right frames, and visually "multiply" it by the electronic wave function from Fig. 2 left frame. The resulting total molecular wave function is single valued everywhere and its permutation symmetry is always correct: in the case of A_1 symmetry it is symmetric and in the case of A_2 symmetry it is antisymmetric across the $\phi=\{0; 120°; 240°\}$ lines. The drawback of the standard BO approach is also clearly seen here: if any BO vibrational wave function (left frames in Fig. 10) is multiplied by the electronic wave function (left frame in Fig. 2) the resulting total molecular wave function is double valued with inconsistent permutation symmetry. Concerning the nodal structure of the GBO wave functions, in the wave function of A_1

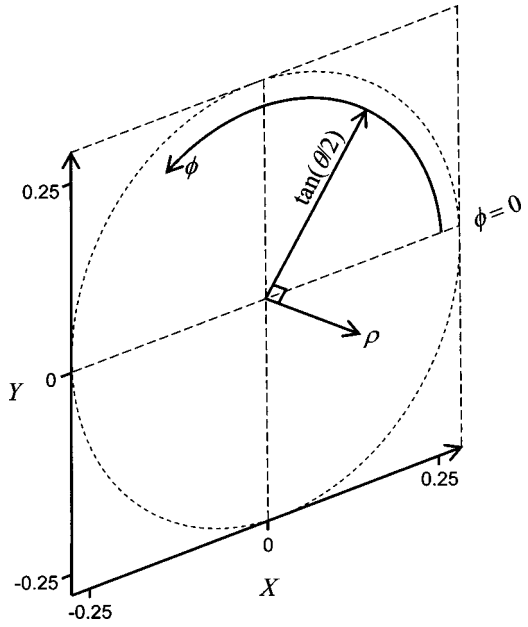

FIG. 6. Schematic of the hyperspherical coordinates used in Figs. 3–5 and 7–9. Orientation of the (x,y)-plane is the same as in all those figures. Hyperradius ρ is plotted in the direction perpendicular to the (x,y) plane.

symmetry the geometric phase *imposes* three additional nodes along the ϕ coordinate at $\phi=\{60; 180°; 300°\}$, while in the wave function of A_2 symmetry it *cancels* the three nodes (see Fig. 10).

In the GBO calculations (as seen from the Fig. 10, right panel) the lowest energy wave functions of A_1 and A_2 symmetries look very similar except that one of them is twisted by $\phi=60°$ around the ρ axis. Thus, the nodes of the A_1 symmetry state coincide with the maxima of the A_2 symmetry state, and vice versa. The three maxima of the A_1 symmetry state are located above the three wells, while the three maxima of the A_2 symmetry state are located above the three transition states. This difference makes the energy of the A_2 state slightly higher ($\sim$101 cm^{-1}) than the energy of the A_1 state. Such a similarity exists between several other GBO states of A_1 and A_2 symmetries and we let the readers find relevant frames in Figs. 7 and 8. Using the 3D plots in Figs. 7–9 the assignments of the GBO vibrational states are straightforward for most of the states, except for the two *E*-symmetry states: 15 and 16. The assignments in terms of the normal mode quantum numbers are given in the sixth column in Tables I–III.

VII. GEOMETRIC PHASE EFFECTS

It appears that the geometric phase not only changes the number of nodes and shifts the energies, but also affects the *order* of the vibrational states.[19,20] For example, among the A_1 symmetry states obtained from the BO calculations the (0,0,2) state is the first excited, the (0,1,0) state is the second excited, and the (1,0,0) state is the fifth excited state. In the GBO results the order is different: the three lower excited states are (0,1,0), (0,0,2), and (1,0,0) in the order of increasing energy. To account for such reorderings we have found for each GBO state in the fifth column in the Tables I–III the corresponding BO state in the second column in the Tables I–III and gave its number in the sixth column of each table. Then we have calculated energy differences between the corresponding GBO and BO states and those are listed in the last column in the Tables I–III. These differences represent the magnitude of the geometric phase effect for each vibrational state and it is very clear that the effect is always positive for the vibrational states of A_1 symmetry and is always negative for the states of A_2 symmetry. As we have demonstrated in the preceding section (see Fig. 10), the geometric phase imposes three nodes in the wave functions of A_1 symmetry and cancels three nodes in all wave functions of A_2 symmetry. Since the number of nodes in the eigenfunction is proportional to the energy of the vibrational state, this explains why all A_1 eigenvalues go up at the same time as all A_2 eigenvalues go down when we include the geometric phase. Because of such shifts the energies of the corresponding states of A_1 and A_2 symmetries in the GBO calculations approach each other, relative to the BO calculations, and become quite close. We have already pointed out that the energy difference between the ground vibrational states of both symmetries, the (0,0,0) A_1 state and the (0,0,1) A_2 state, is only $\sim$101 cm^{-1} in the GBO calculations in contrast with $\sim$477 cm^{-1} in the BO calculations. Similarly, the eigenvalues of many other states of A_1 and A_2 symmetries are brought closer together in the GBO calculations (compare Tables I and II) relative to BO calculations. Recall that in the preceding section, we showed that the corresponding wave functions in such cases become very similar too (they are just twisted by $\phi=60°$).

In the case of *E* symmetry (see Table III), we obtain both positive and negative shifts due to the geometric phase effects and their magnitudes are generally smaller than those in the states of A_1 and A_2 symmetries. However, there is an important qualitative change related to *E*-symmetry states. In the standard BO calculations, the lowest energy state is always the A_1 symmetry state (0,0,0). However, in the GBO calculations the lowest energy state is the ground vibrational state of *E* symmetry. It is $\sim$75 cm^{-1} below the corresponding state of A_1 symmetry. This reversal of the symmetry of the ground vibrational state is well known and, probably, was the first experimentally verified example of a geometric phase effect.[12–14,30]

Overall, the geometric phase effects in the case of cyclic-N_3 are very large: Among the A_1 symmetry states it is only the ground vibrational state (0,0,0) that is shifted by less then 100 wave numbers ($\sim$91 cm^{-1}) compared to the standard BO result. Other A_1 states are shifted more significantly with the largest energy shift of $\sim$609 cm^{-1} for the state (0,0,4). The smallest energy shift for A_2 symmetry states is almost 300 wave numbers ($\sim$286 cm^{-1}) for the ground vibrational state (0,0,1) and the largest is $\sim$642 cm^{-1} for the state (0,0,5). The shifts of the *E*-symmetry states are between $\sim$39 cm^{-1} for the ground (0,0,0) state and $\sim$221 cm^{-1} for (0,0,6) state. By analyzing the Tables I–III. We conclude that the larger shifts are observed for the states with the larger asymmetric stretch quantum numbers v_3. This is because such states have a larger number of nodes along the ϕ coordinate, so that adding or removing the three geometric phase

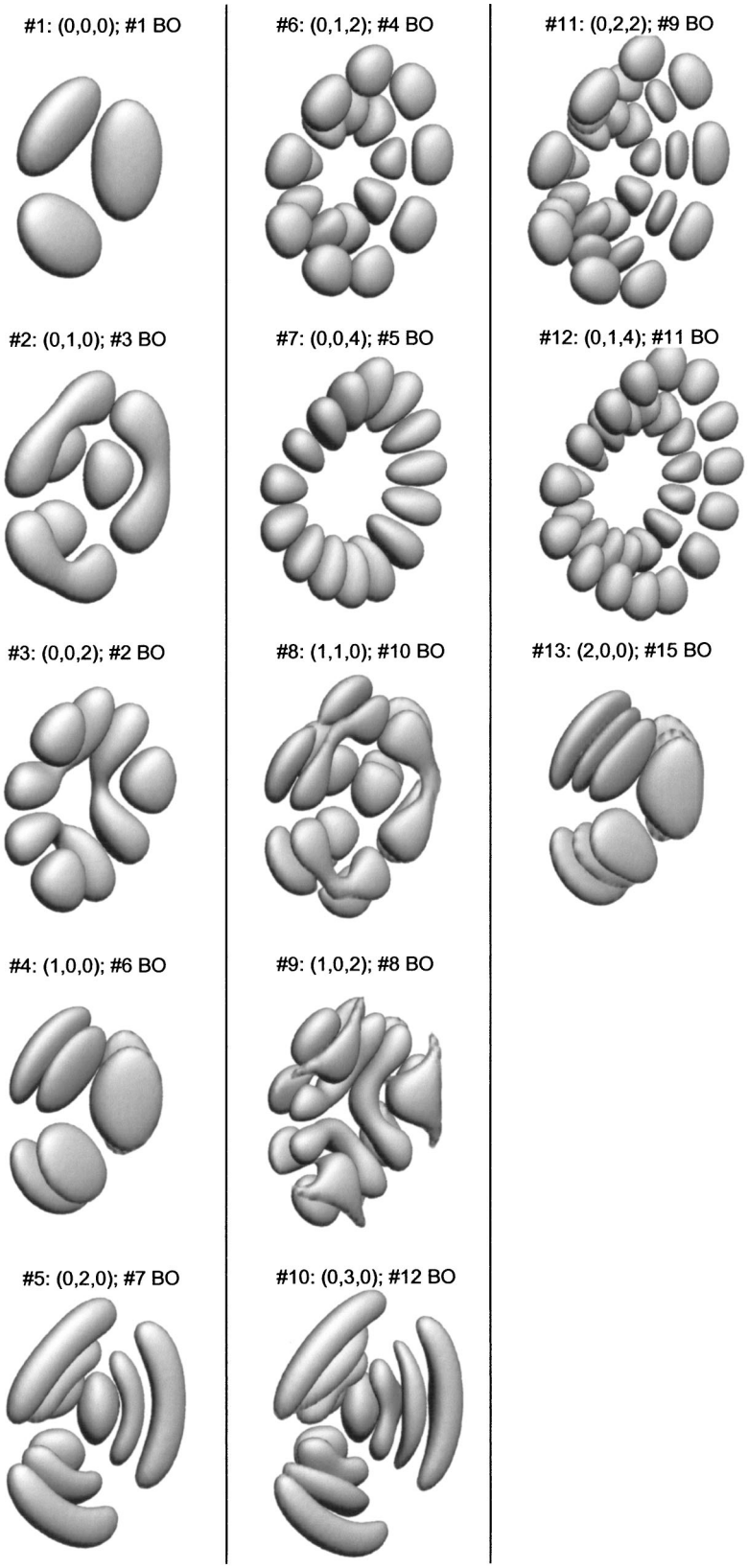

FIG. 7. Three-dimensional wave functions for GBO vibrational eigenstates of A_1 symmetry in cyclic-N_3. Assignment is given on top of each wave function, together with the state number of the corresponding BO wave function in Fig. 3.

nodes along ϕ affects these states more significantly. On average, these geometric phase effects are about two orders of magnitude larger than those reported earlier for Na_3 molecule (see Table I in Ref. 20). We believe that this is due to the rare coincidence: the zero-point energy of cyclic-N_3 is very large and, at the same time, its pseudorotation barrier is very low. It is for this reason the wave function of the BO ground vibrational state is almost isotropic in ϕ and looks very similar to a torus.

In Table IV we give the fundamental frequencies of cyclic-N_3 obtained from both the BO and the GBO calculations. This table makes it obvious that the character of the

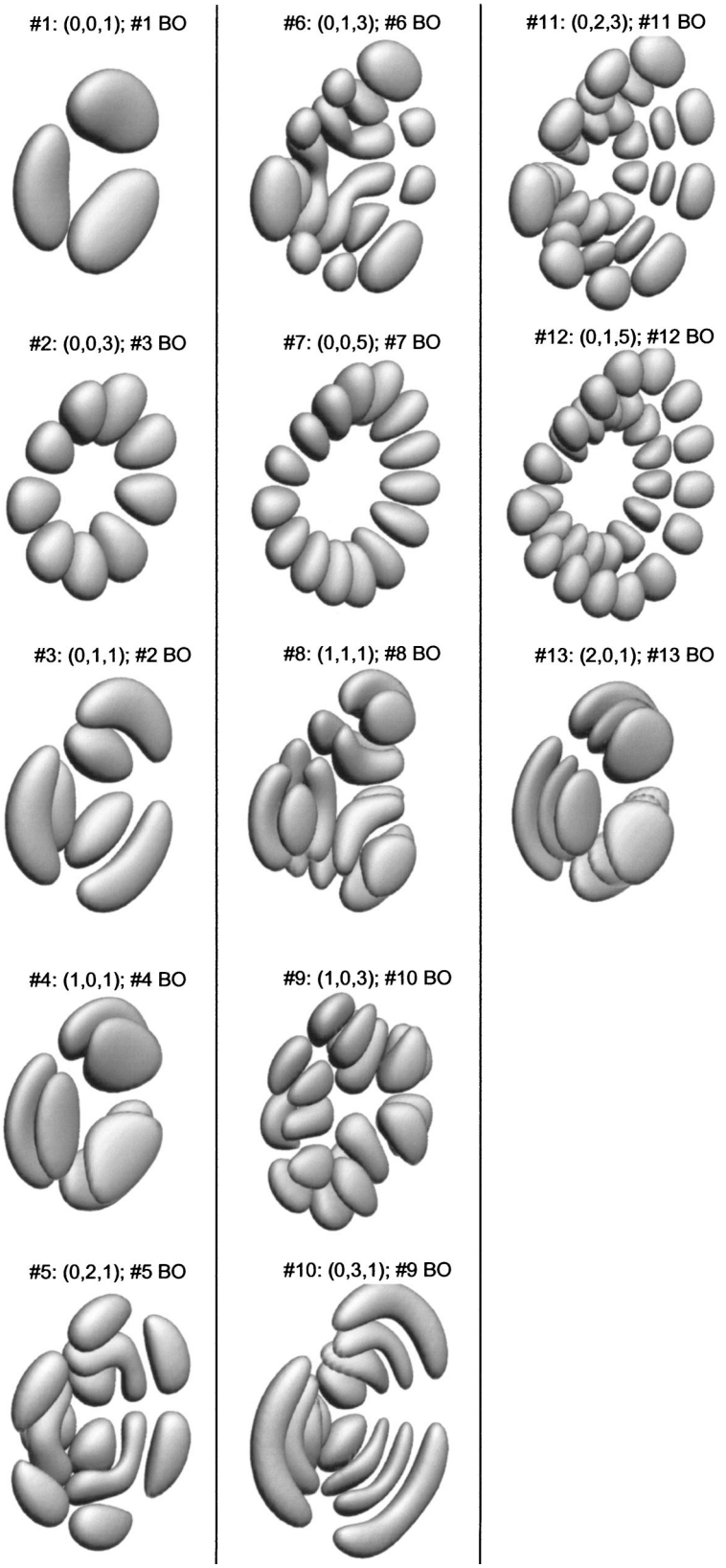

FIG. 8. Three-dimensional wave functions for GBO vibrational eigenstates of A_2 symmetry in cyclic-N_3. Assignment is given on top of each wave function, together with the state number of the corresponding BO wave function in Fig. 4.

vibrational spectra in the cyclic-N_3 is significantly affected by the geometric phase effects. The v_1 and v_2 modes of each symmetry are brought closer together (compared to the standard BO results), especially in the case of A_1 symmetry, where the GBO v_1 and v_2 modes are different by less then 8 cm^{-1} (compared to $\sim$319 cm^{-1} in the BO case). Also note, that the order of v_1 and v_2 modes is reversed in the GBO results (compared to the BO results) for both the A_1 and A_2 symmetries. In the last column of Table IV, we give the frequency shifts due to the geometric phase effects. As expected, the frequency shifts are larger for asymmetric stretch normal modes v_3 of all symmetries. For all modes of A_1

symmetry the shifts are positive and for all modes of A_2 symmetry the shifts are negative.

As we have already explained in the preceding section, the $\ell=6$ generalized BO results should (theoretically) be identical to the standard BO results, so that the difference (if there is any) is a signal of numerical errors associated with the involvement of the gauge potential terms into the Hamiltonian. We have computed such differences for each state and they are given in the fourth column in the Tables I–III. For all states of A_2 symmetry these errors are very small: less then 0.1 cm^{-1} (see Table II). They are also quite small, less then 0.6 cm^{-1} for all states of E symmetry (see Table III). For most states of A_1 symmetry the errors are also about one wave number, but there are few exceptions: states 6, 7, 10, 12, 15, and 17 exhibit errors between the 3 and 30 cm^{-1} (see Table I). We note that these are the same states where

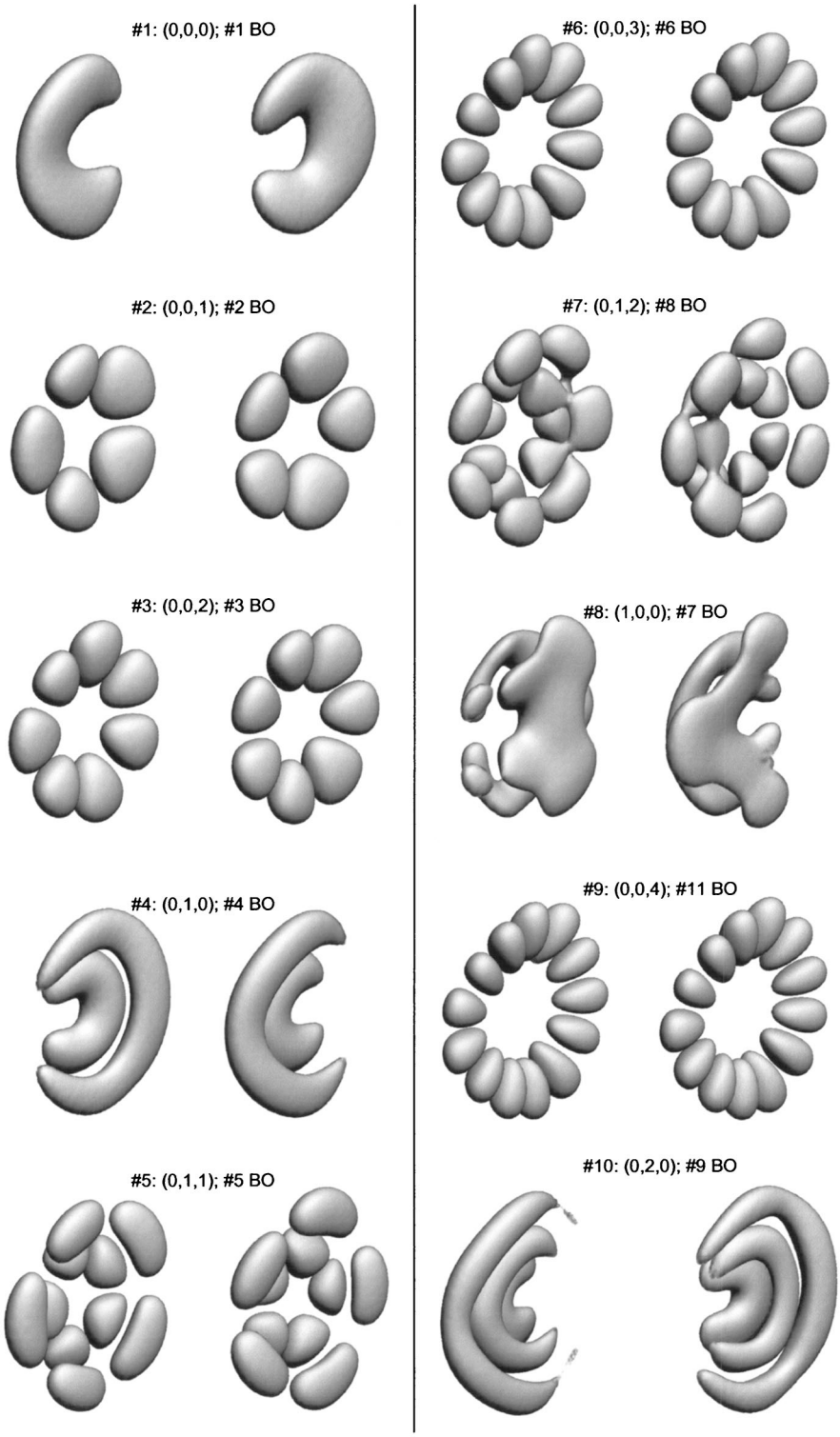

FIG. 9. Three-dimensional wave functions for GBO vibrational eigenstates of E symmetry in cyclic-N_3. Assignment is given on top of each wave function, together with the state number of the corresponding BO wave function in Fig. 5.

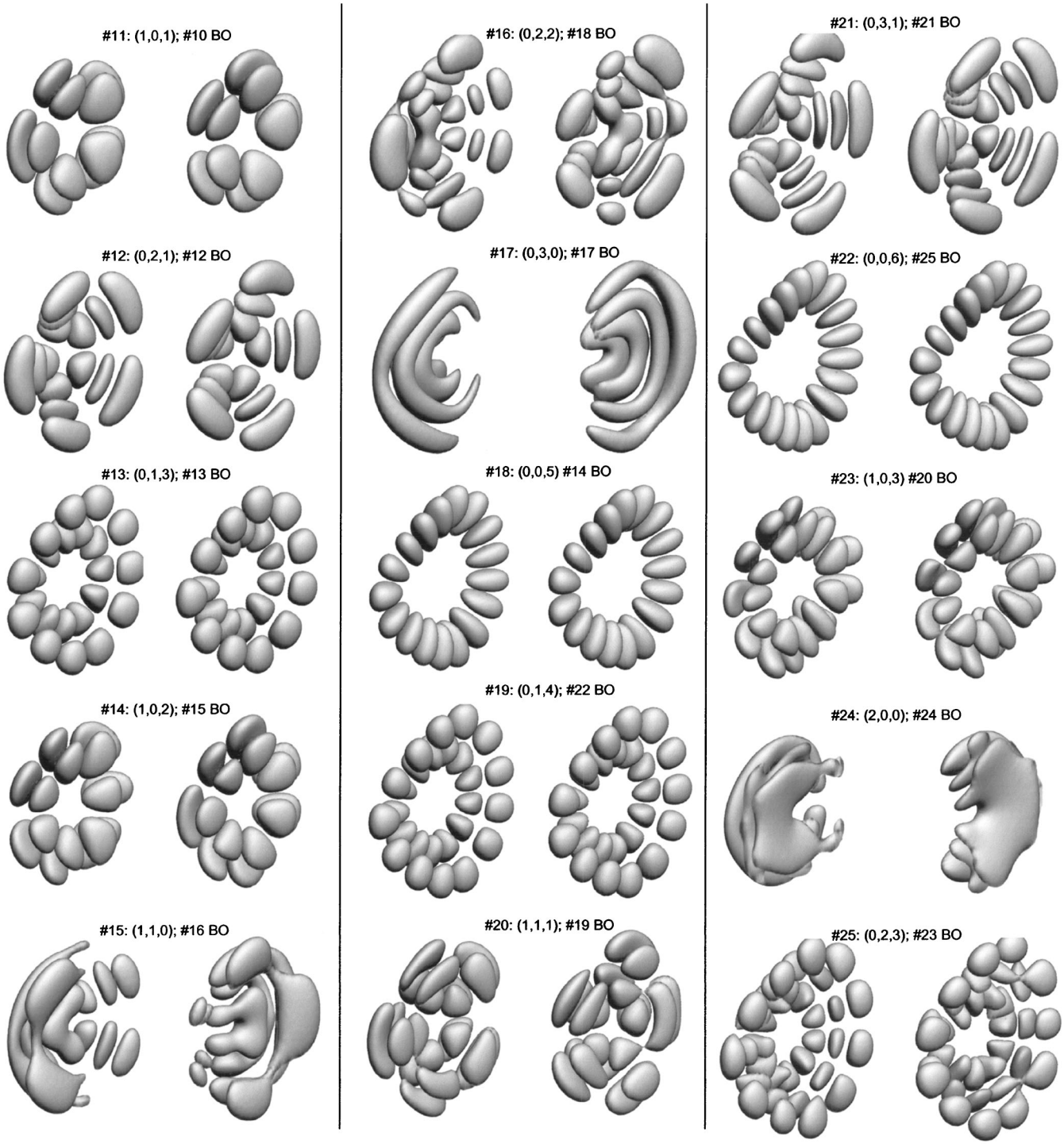

FIG. 9. (*Continued*.)

the BO wave function exhibits nonzero amplitude at the origin, $\theta=0$ (see Fig. 3). We also recall that the GBO Hamiltonian in Eq. (24) is singular at $\theta=0$ as shown in Eqs. (27)–(28). It is because of these singularities that our $\ell=6$ generalized BO calculations cannot reproduce perfectly the standard BO wave functions near the $\theta=0$. Even a dramatic increase of the basis set size in θ produces only tiny improvements. These singularities can, in principle, be accurately treated in the same way as we treat the Eckart singularities: by the appropriate choice of the basis set functions.[41] An accurate treatment of these singularities will be required for calculations of the vibrational states at energies above the conical intersection, especially for cone states which exhibit large amplitude very close to the origin $\theta=0$. We plan to undertake such developments in the future. In the present study, we consider energies below the conical intersection and found no GBO states that exhibit large amplitude at the origin (for a general proof of this property see the Ref. 46). This is readily checked by inspecting the $\theta=0$ region of all the GBO wave functions in the Figs. 7–9. A question arises:

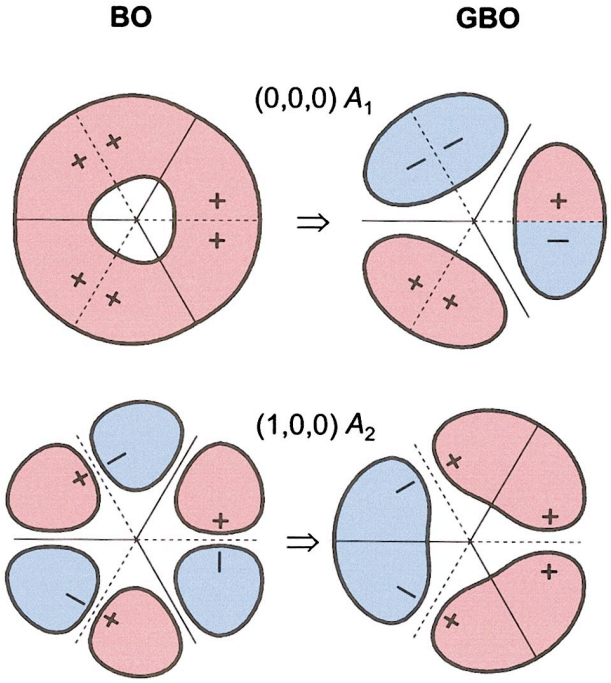

FIG. 10. (Color) Demonstration of the changes in the nodal structure of vibrational wave functions due to the geometric phase effects. The wave functions obtained from BO and GBO calculations for the (0,0,0) state of A_1 symmetry and the (0,0,1) state of A_2 symmetry are shown. The BO wave functions are single-valued everywhere. The GBO wave functions change sign, which is seen at $\phi=0$ as a sharp red-blue boundary for A_1 symmetry state and a (+/+) node of A_2 symmetry state. When the GBO vibrational wave function (A_1 or A_2) is multiplied by the electronic wave function (Fig. 2, left panel), the total molecular wave function is single-valued with the correct permutation symmetry everywhere. See text for further details.

what is so special about those few BO states of A_1 symmetry (6, 7, 10, 12, 15, and 17) that exhibit nonzero probability at the origin? It appears that those few states (and also the BO states 1 and 3 of A_1 symmetry) are the only states in Figs. 3–5 and 7–9 that exhibit no nodes along the ϕ coordinate. Indeed, all the GBO states in Figs. 7–9 are required to have at least the three geometric phase nodes. All the A_2 and E symmetry BO states in Figs. 4–5 are required to have nodes by symmetry. Among the BO states of A_1 symmetry those that have at least one quantum of asymmetric stretch v_3 are also required to have the nodes along the ϕ coordinate. What remains are eight $v_3=0$ states of A_1 symmetry (BO) that exhibit no nodes in ϕ. Among them the two low-lying states (1 and 3) stay far away from the origin just because they are not excited enough. Finally, we are left with the six excited BO states of A_1 symmetry that have $v_3=0$ and exhibit no nodes in ϕ. Now we note that any wave function that exhibits nodes in ϕ is required to vanish at the origin ($\theta=0$) because it changes sign when the observer passes through the origin (through the conical intersection). This is clearly seen in the Fig. 10 (left lower panel, for example). That is why the majority of states reported in this paper vanish at the origin (due to symmetry), so that the singularities of the GBO Hamiltonian (24) do not cause any practical difficulty. The singularity problem is seen only in those six BO states of A_1 symmetry that are not required to vanish at zero since they are $v_3=0$ states and have no nodes in ϕ. Because the errors are still small for most of the states and all the BO states are considered here only for comparison (the BO states are wrong anyway) the singularities cause no problems whatsoever in the present study.

TABLE IV. BO and GBO fundamental frequencies in cyclic-N_3.

Vibrational symmetry	Normal mode	BO frequencies (cm^{-1})	GBO frequencies (cm^{-1})	Geometric phase shifts (GBO-BO)(cm^{-1})
A_1	v_1	1546.20	1602.45	56.25
	v_2	818.31	861.09	42.78
	v_3	499.42	868.71	369.29
A_2	v_1	1611.72	1536.51	−75.21
	v_2	886.07	837.47	−48.60
	v_3	1038.88	770.70	−268.18
E	v_1	1566.54	1562.57	−3.97
	v_2	842.19	825.82	−16.37
	v_3	195.73	343.21	147.48

VIII. CONCLUSIONS

The study of the vibrational spectra for the cyclic-N_3 molecule was presented. This study included the standard BO calculations as well as the generalized BO calculations, where the geometric phase effects due to the D_{3h} conical intersection are taken into account using the gauge theory approach. By comparing the results of these two approaches, we have shown that the standard BO results, where the geometric phase is totally neglected, are not even qualitatively correct in the case of cyclic-N_3. The shifts of the vibrational eigenvalues (due to the geometric phase effects) are unusually large and exceed 600 cm^{-1} for several states. Since even the ground vibrational states of the cyclic-N_3 are formed at energies well above the pseudorotation barriers, the geometric phase affects these states too, especially the lowerst energy state of A_2 symmetry where the shift due to the geometric phase is as large as 286 cm^{-1}. Significant changes have been observed not only in the positions, but also in the order of the vibrational states and in the ordering of the fundamental frequencies. Such adverse changes should clearly be seen in the experimental spectra and we are looking forward to the possibility of a direct comparison of the theoretical predictions and experimental measurements, which may become available in the near future.[2–5]

From the theory perspective the cyclic-N_3 offers many more opportunities. At energies close to the energy of the conical intersection the non-adiabatic effects due to interaction with the excited electronic state may become important. Theoretical studies of such states will require knowledge of the excited state PES as well as the nonadiabatic couplings between the two surfaces. At the point of conical intersection, an accurate treatment of the singular terms in the GBO. Hamiltonian (as described in the poreceding section) and of the singularities in the nonadiabatic coupling matrix[43] is required. Nonadiabatic calculations are more difficult and will require significant additional developments.[44] However, they are important, since the spectral range around the conical

intersection and above it ($\omega \geqslant 3000$ cm^{-1}) is easy to probe experimentally. We plan to purse such calculations in the future.

ACKNOWLEDGMENT

The authors would like to thank Professor Alec Wodtke, University of California at Santa Barbara, for bringing the subject of cyclic-N_3 to the attention of our theoretical groups.

[1] M. Bittererova, H. Ostmark, and T. Brink, J. Chem. Phys. **116**, 9740 (2002).
[2] N. Hansen, A. M. Wodtke, A. V. Komissarov, and M. C. Heaven, Chem. Phys. Lett. **368**, 568 (2002).
[3] N. Hansen and A. M. Wodtke, J. Phys. Chem. A **107**, 10608 (2003).
[4] N. Hansen, A. V. Komissarov, K. Morokuma, M. C. Heaven, and A. M. Wodtke, J. Chem. Phys. **118**, 10485 (2003).
[5] D. Matsiev, J. Chen, M. Murphy, and A. M. Wodtke, J. Chem. Phys. **118**, 9477 (2003).
[6] P. Zhang, K. Morokuma, and A. M. Wodtke, J. Chem. Phys. (to be published).
[7] D. Babikov, P. Zhang, and K. Morokuma, J. Chem. Phys. **121**, 6743 (2004).
[8] G. Herzberg and H. C. Longuet-Higgins, Discuss. Faraday Soc. **35**, 77 (1963).
[9] C. A. Mead and D. G. Truhlar, J. Chem. Phys. **70**, 2284 (1979); C. A. Mead, *ibid*. **72**, 3839 (1980).
[10] C. A. Mead, Chem. Phys. **49**, 23 (1980).
[11] M. V. Berry, Proc. R. Soc. London, Ser. A **392**, 45 (1984).
[12] F. S. Ham, Phys. Rev. Lett. **58**, 725 (1978).
[13] M. C. M. O'Brien, Proc. R. Soc. London, Ser. A **281**, 323 (1964).
[14] R. E. Coffman, Phys. Rev. Lett. **19**, 475 (1965); **21**, 381 (1965); J. Chem. Phys. **48**, 609 (1968).
[15] H. C. Longuet-Higgins, U. Opik, M. H. L. Pryce, and R. A. Sack, Proc. R. Soc. London, Ser. A **224**, 1 (1958).
[16] W. H. Gerber and E. Schumacher, J. Chem. Phys. **69**, 1692 (1978).
[17] T. C. Thompson, D. G. Truhlar, and C. A. Mead, J. Chem. Phys. **82**, 2392 (1985).
[18] D. G. Truhlar, T. C. Thompson, and C. A. Mead, Chem. Phys. Lett. **127**, 287 (1986).
[19] B. K. Kendrick, Phys. Rev. Lett. **79**, 2431 (1997).
[20] B. K. Kendrick, Int. J. Quantum Chem. **64**, 581 (1997).
[21] H. von Busch, V. Dev, H. A. Eckel, S. Kasahara, J. Wang, W. Demtröder, P. Sebald, and W. Meyer, Phys. Rev. Lett. **81**, 4584 (1998).
[22] M. Keil, H.-G. Krämer, A. Kudell, M. A. Baig, J. Zhu, W. Demtröder, and W. Meyer, J. Chem. Phys. **113**, 7414 (2000).
[23] M. Mayer and L. S. Cederbaum, J. Chem. Phys. **105**, 4938 (1996).
[24] R. Meiswinkel and H. Köppel, Chem. Phys. **144**, 177 (1990).
[25] J. Schön and H. Köppel, Chem. Phys. Lett. **231**, 55 (1994).
[26] J. Schön and H. Köppel, J. Chem. Phys. **103**, 9292 (1995).
[27] B. Lepetit and A. Kuppermann, Chem. Phys. Lett. **166**, 581 (1990).
[28] B. K. Kendrick, J. Phys. Chem. A **107**, 6739 (2003).
[29] B. K. Kendrick, in *Conical Intersections: Electronic Structure, Dynamics and Spectroscopy*, Geometric Phase Effects in Chemical Reaction Dynamics, edited by W. Domcke, D. R. Yarkony, and H. Köppel (World Scientific, Singapore, 2004).
[30] C. A. Mead, Rev. Mod. Phys. **64**, 51 (1992).
[31] D. R. Yarkony, Rev. Mod. Phys. **68**, 985 (1996).
[32] B. K. Kendrick and R. T Pack, J. Chem. Phys. **104**, 7475 (1996).
[33] B. K. Kendrick and R. T Pack, J. Chem. Phys. **104**, 7502 (1996).
[34] B. K. Kendrick and R. T Pack, J. Chem. Phys. **106**, 3519 (1997).
[35] B. K. Kendrick, J. Chem. Phys. **112**, 5679 (2000); **114**, 4335(E) (2001).
[36] B. K. Kendrick, J. Chem. Phys. **118**, 10502 (2003).
[37] H.-J. Werner and P. J. Knowles, MOLPRO Version 2002.1, with contributions from R. D. Amos, A. Bernhardsson, A. Berning *et al*.
[38] H.-J. Werner and P. J. Knowles, J. Chem. Phys. **89**, 5803 (1988).
[39] E. R. Davidson, J. Comput. Phys. **17**, 87 (1975).
[40] R. T Pack and G. A. Parker, J. Chem. Phys. **87**, 3888 (1987).
[41] B. K. Kendrick, R. T Pack, R. B. Walker, and E. F. Hayes, J. Chem. Phys. **110**, 6673 (1999).
[42] C. de Boor, *A Practical Guide to Splines* (Springer, New York, 1978).
[43] B. K. Kendrick, C. A. Mead, and D. G. Truhlar, Chem. Phys. **277**, 31 (2002).
[44] A. W. Jasper, B. K. Kendrick, C. A. Mead, and D. G. Truhlar, in *Modern Trends in Chemical Reaction Dynamics*, Non-Born–Oppenheimer Chemistry: Potential Surfaces, Couplings and Dynamics, edited by X. Yang and K. Liu (World Scientific, Singapore, 2004).
[45] B. R. Johnson, J. Chem. Phys. **67**, 4086 (1977); **68**, 4678 (1978).
[46] C. A. Mead, J. Chem. Phys. **78**, 807 (1983).